M. Schäferling

DOI: 10.1002/anie.201105459

Chemical Sensors

The Art of Fluorescence Imaging with Chemical Sensors

*Michael Schäferling**

Keywords:
dyes/pigments · fluorescence imaging · fluorescent probes · luminescence · materialssciencesensors

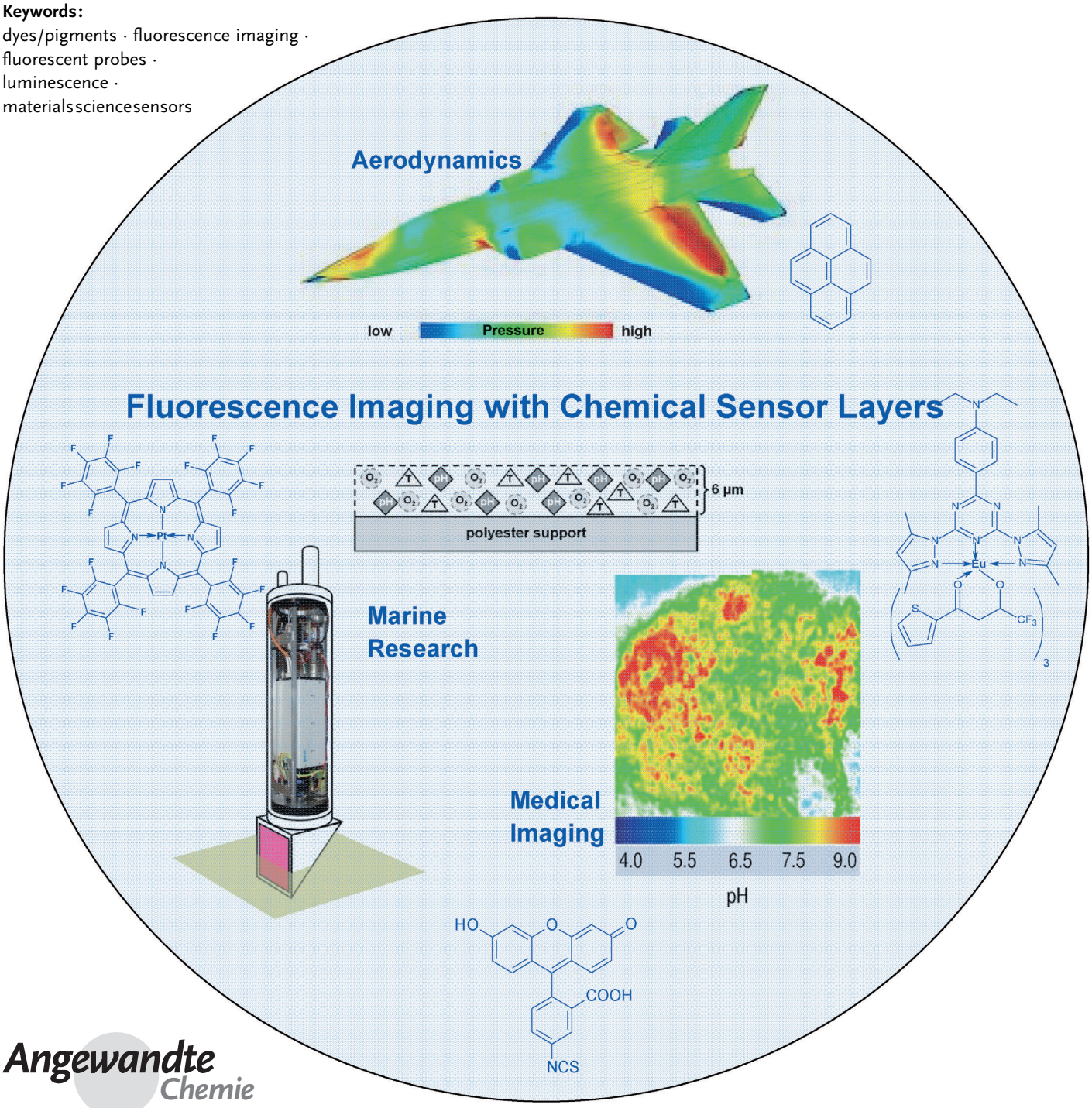

Angewandte International Edition Chemie

Fluorescence imaging techniques involving chemical sensors are essential tools in many fields of science and technology because they enable the visualization of parameters which exhibit no intrinsic color or fluorescence, for example, oxygen, pH value, CO_2, H_2O_2, Ca^{2+}, or temperature, to name just a few. This Review aims to highlight the state of the art of fluorescence sensing and imaging, starting from a comprehensive overview of the basic functional principles of fluorescent probes (or indicators) and the design of sensor materials. The focus is directed towards the progress made in the development of multiple sensors and methods for their signal read out. Imaging methods involving optical sensors are applied in quite diverse scientific areas, such as medical research, aerodynamics, and marine research.

From the Contents

1. Introduction

Molecular imaging is a highly important tool in life sciences and engineering. The generic term comprises analytical methods such as advanced X-ray methods (computer tomography), positron emission tomography, magnet resonance imaging, and scanning probe microscopy. These techniques enable the high-contrast imaging of organs or soft tissue and paved the way to analyze material surfaces at the molecular level. Biomedical optical imaging mainly involves fluorescence microscopy. Sectional views can be obtained with confocal microscopes if tissue, cells, or cellular compartments are stained with fluorescent dyes. Biomolecules can also be selectively labeled with fluorescent dyes to monitor biomolecular interactions inside cells or at transmembrane-bound receptors. Staining and labeling techniques for fluorescence microscopy have been reviewed extensively in the past few years.[1]

Fluorophores can not only be used to label molecules or stain cells, they can also act as an indicator (or "probe") to determine intrinsically nonfluorescent species and parameters such as pH value, oxygen, or metal ions. In the latter case, their photoluminescent properties (fluorescence or phosphorescence intensity, anisotropy, lifetime, or emission wavelength) respond to the chemical composition of the environment. Fluorescence quenching is only one approach in the application of dyes for chemical sensing and imaging. Fluorogenic probes can also be designed that exhibit luminescence amplification during the course of a chemical reaction. These "turn on" probes have distinct advantages compared to quenchable probes. Dual-wavelength (2-λ) probes are another useful type of sensitive dyes because these can be applied to intrinsically referenced assays. They undergo a shift in their absorption and/or emission maxima on protonation or formation of a complex with metal ions. These strategies will be highlighted in Section 3 of this Review.

Sections 4 and 5 address sensor materials for imaging applications. Typically, chemical sensors exhibit two characteristics:

a) they contain two basic components connected in series: a chemical or molecular recognition system (receptor) and a physicochemical transducer;[2] and
b) they are miniaturized devices that can deliver real-time and on-line information on the presence of specific compounds or ions even in complex samples.[3]

Luminescent probes have the advantage that they can be delivered directly into the sample—now often encapsulated in nanoparticles—and detected by a remote monitoring mode. Accordingly, optical chemical sensors consist of the recognition unit (in some cases, however, the chromophore acts as both the receptor and the transducer), a light source, and a photodetector, which is usually a charge-coupled device (CCD) camera in imaging techniques.

Fluorescence sensor materials mostly consist of a polymeric support or binding matrix, which incorporates the indicator and is permeable to the analyte. They can be used for imaging, and be integrated in fiberoptic (micro)sensors, microtiter plates, or sensor arrays.[4] Their applications include process control (e.g. on-line monitoring of (bio)-chemical reactors), pharmaceutical screening (including detection of enzymatic reactions or cell respiration), and the determination of blood gases and electrolytes, such as O_2, CO_2, Ca^{2+}, and K^+, as well as the pH value.[5] Optical chemical sensors have been reviewed frequently in the past few years.[6] This Review focuses on fluorescence probes and materials used in sensor layers or nanoparticles for chemical imaging. Particular attention is paid to recent developments in multiple

[*] Priv.-Doz. Dr. M. Schäferling
Institute of Analytical Chemistry, Chemo- and Biosensors
University of Regensburg
93040 Regensburg (Germany)
E-mail: michael.schaeferling@chemie.uni-regensburg.de

sensors that respond to various species with differentiable output signals. The most important parameters addressed are partial oxygen pressure (pO_2), barometric pressure, pH value, temperature, H_2O_2, and metal ions such as Ca^{2+}. Moreover, enzymatic activity can be visualized with probes that are sensitive to pO_2, pH, or H_2O_2.

2. Fluorescence Imaging: Methods and Requirements

The instrumentation for sensory imaging consists of three parts, namely

a) an indicator or a sensor layer,
b) an optoelectronic system that records the photoluminescence of the indicator or sensor layer, and
c) a computer-aided control unit for the optoelectronic system along with software for image processing.

Optoelectronic imaging systems span applications from the microscopic to the macroscopic level. Hence, they can be used to obtain user-defined levels of complexity, and can be connected, for example, to confocal microscopes or fast-pulsed time-resolved measurement techniques. They require a light source—such as a halogen lamp, an array of light-emitting diodes (LEDs), or laser diodes—and a system of optical filters which separates the short-wavelength excitation light from the long-wavelength luminescent light. Compact instruments include a beam splitter (dichroic mirror), which reflects the short-wavelength excitation light in the direction of the sample and transmits the long-wavelength luminescence to the detector. Two basic approaches are used: laser scanner and imaging systems. The scanning principle is realized in confocal microscopes and in microarray readers. Generally, scanners are equipped with several lasers for different excitation wavelengths, a movable x/y stage, and a photomultiplier tube (PMT) as the detector. A typical imaging system consists of a CCD camera as the detector element and a LED array or white light source in combination with a set of appropriate optical filters (Figure 1).

The imaging of fluorescent sensors is accompanied by problems such as photobleaching of the applied dyes, light scatter, background fluorescence of the sample, inhomogeneous illumination, instability of the light source, non-uniform distribution of the fluorescent probes in the sample or the sensor layer, and a varying thickness of the sensor layer. Hence, the optical sensor system has to be thoroughly calibrated and referenced. Intrinsically referenced methods are of particular interest in fluorescence sensor technology and have been reviewed recently.[7] They enable the elimination of the interferences specified above and can simplify calibration procedures. Generally, referencing is based on ratiometric measurements. These include the addition of reference dyes which behave inertly towards the respective analyte or the application of 2-λ probes. These approaches will be discussed in the next section.

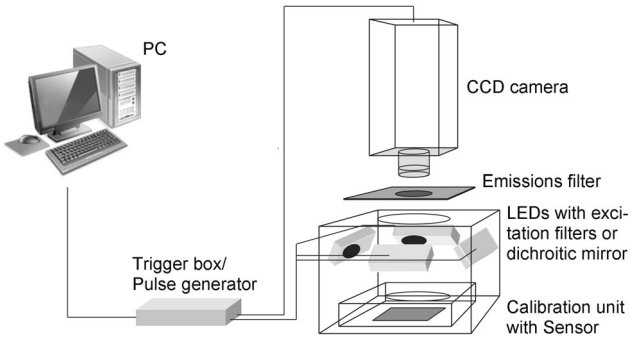

Figure 1. Time-resolved fluorescence imaging system for the calibration and read out of optical chemical sensors.

Alternatively, internally referenced techniques can be employed, such as fluorescence lifetime imaging (FLIM). FLIM records the lifetime of the excited electronic state of a fluorophore, and is probably the most attractive intrinsically referenced parameter. The decay of the fluorescence intensity after a short pulse of light is monoexponential in the ideal case [Eq. (1)]. I_0 is the intensity at $t=0$ and τ is the

$$I = I_0 \exp^{-t/\tau} \quad (1)$$

fluorescence lifetime (or decay time). This is the time that is required until the fraction of molecules in the excited state has decreased to $1/e$. The fluorescence lifetime is not affected by the concentration of the fluorophores, static quenching effects, or the brightness of the light source. In contrast, dynamic quenching, resonance energy transfer, and temperature have a strong impact on the fluorescence decay. Thus, the fluorescence lifetime is a preferred parameter in fluorescence sensing and imaging.

Methods for the determination of the lifetime can be classified into time-domain and frequency-domain approaches.[8] The latter is based on a phase-modulation technique, in which the sensor is excited with sinusoidally modulated light at a frequency approximately reciprocal to the decay time. The emission of the probe follows the modulation, but with a certain delay. This is measured as a change of the phase angle. Accordingly, τ can be calculated from the phase angle or the modulation ratio. Phase fluorimetry is widely used in fiberoptic sensors but hardly applicable to imaging, and thus will be not discussed in more

Dr. Michael Schäferling completed his chemistry diploma in 1997 at the University of Ulm, where he also obtained his PhD in 2001 with Prof. Peter Bäuerle. 2000–2002 he was project leader for the development of DNA and protein microarrays at Thermo Hybaid GmbH in Ulm, before becoming research assistant to Prof. Otto S. Wolfbeis at the Institute of Analytical Chemistry, Chemo- and Biosensors, at the University of Regensburg. In 2008 he finished his Habilitation and was appointed as Associate Professor. From 2013 he will be FiDiPro (Finland Distinguished Professor) fellow at the Department of Biochemistry and Food Chemistry at the University of Turku.

detail here. However, suitable cameras are already in development.

The most frequently used pulsed technique for the determination of luminescence lifetimes is the time-correlated single-photon counting (TCSPC). It is based on the detection of single photons hitting the photodetector after short excitation pulses. The time between the excitation pulse and detection is recorded. The decay curve can be generated in the form of a histogram by integration of many pulses. However, TCSPC requires complex instrumentation, exact synchronization of the modules, and generates extensive data. Therefore, it is not practicable for fluorescence sensing and imaging. Less-intricate time-gated methods are applied for FLIM. A straightforward approach termed Rapid Lifetime Determination (RLD)[9] records the fluorescence intensity in two successive time gates. These are set within certain delays after a short pulse of the excitation light (Figure 2).

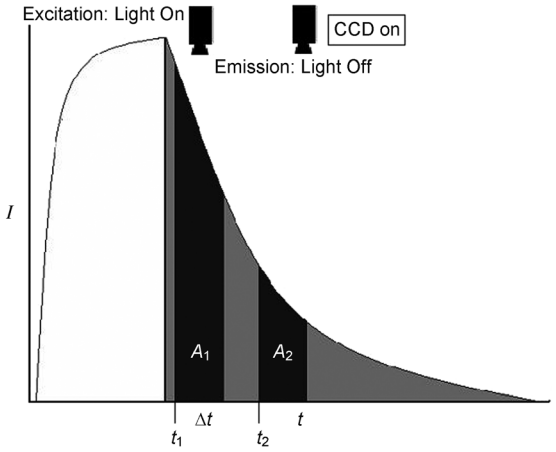

Figure 2. The change in the fluorescence lifetime τ can be accessed by the rapid lifetime determination method with time-gated detection. The detector is opened after a short pulse of light at times t_1 and t_2 for an identical period of Δt. The lifetime is proportional to the ratio of the integrated photon counts A_1 and A_2.

In the case of a monoexponential decay and an identical length of the time gates Δt, the lifetime τ can be calculated according to Equation (2), where Δt is the width of the

$$\tau = \frac{\Delta t}{\ln(A_1/A_2)} \qquad (2)$$

respective integration intervals A_1 and A_2. RLD is not very accurate in terms of calculating absolute lifetimes, particularly in the case of multiexponential fluorescence decays, because of its origin in just two images at different delay times. The precision of this method is dependent on the integration times, which have to be set in a proper relationship with the lifetime ($\Delta t/\tau \approx 2$) and a sufficient number of photon counts.[10] Overlapping integrals have to be selected in the case if higher ratios of $\Delta t/\tau$ are required. Double-exponential decays require four integration gates to calculate both the lifetimes and their corresponding preexponential factors.[11]

In practice, the images of the two different gates are taken separately in subsequent acquisition cycles. Therefore, the light source and the detector have to be pulsed at a suitable frequency that is of the same magnitude as the reciprocal decay time. The integration of the two sets of images is followed by a subtraction of the corresponding background dark images that were detected with the same time gates and frequency, but without illumination. The determination of absolute lifetime values is not mandatory for sensor applications. Thus, the significant variable is the change in the ratio $R = A_1/A_2$ as a function of the analyte concentration.

3. Design of Luminescence Probes

Luminescence probes can be configured according to different basic principles, which can be summarized according to the following sensing mechanisms: 1) quenchable probes, 2) fluorogenic probes, 3) dual-wavelength probes, 4) Förster resonance energy transfer (FRET) based probes, and 5) photoinduced electron-transfer (PET) systems.

The functionality of the dye determines the kind of imaging method and its referencing, for example, dual-wavelength or time-resolved measurements, or the addition of reference dyes. This section will provide a closer look at the different kinds of responsive dyes that can be employed in optical sensors and chemical imaging with respect to the most frequently targeted parameters of pH value, pCO_2, pO_2, air pressure, temperature, and metal ions (mainly Ca^{2+} and K^+).

3.1. Fluorescence Probes for pH Sensing

Dual-wavelength probes represent a straightforward and widespread approach to obtain internal referenced optical pH sensors. Two basic strategies can be pursued:

a) detection of fluorescence emission at two different excitation wavelengths, or
b) detection at two different emission wavelengths at a fixed excitation wavelength.

Most instruments for fluorescence analysis, such as microscopes and scanning or imaging devices, are equipped for 2-λ excitation and contain a set of narrow-bandpass filters for the separation of the respective emission wavelengths. Miniaturized low-cost devices specially designed for ratiometric fluorescence measurements have also been configured.[12]

The basic principle of ratiometric pH-sensitive probes can be illustrated by means of 8-hydroxypyrene-1,3,6-trisulfonate (HPTS), a bright fluorophore with a fluorescence quantum yield close to unity and a pK_a value of approximately 7.3 in aqueous solution. The acidic and basic forms of HPTS are shown in Figure 3 along with the resulting excitation and emission spectra.[13] HPTS exhibits a pH-dependent shift of its absorption band. This enables the ratiometric measurement of the fluorescence emission at 520 nm by excitation at both maxima at 405 and 450 nm.

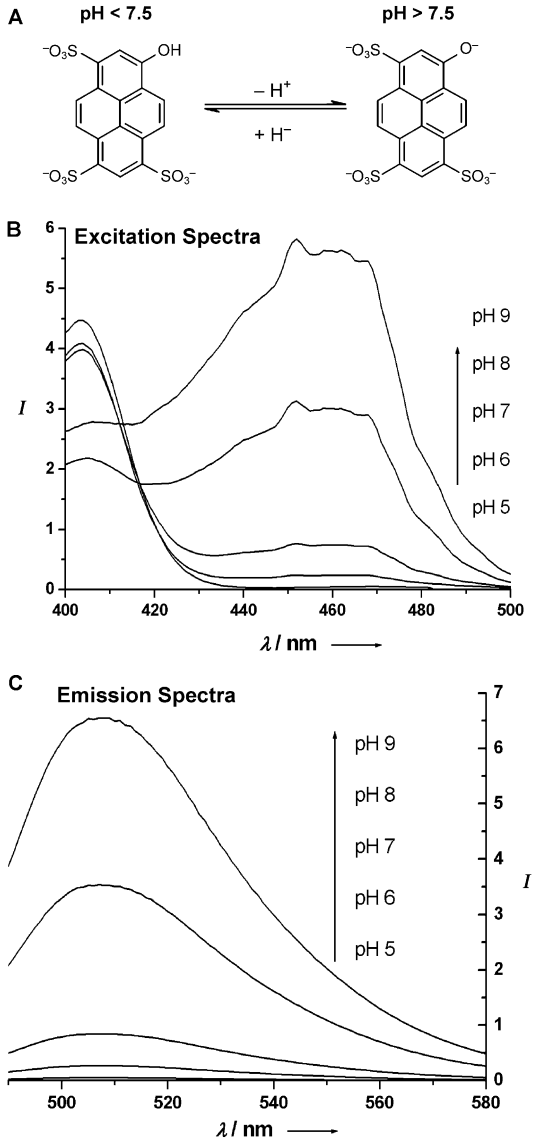

Figure 3. A) Protonated and deprotonated forms of HPTS and B) corresponding excitation (at $\lambda_{em} = 520$ nm) and C) emission ($\lambda_{exc} = 460$ nm) spectra.

The protonated and deprotonated form of some fluorescein derivatives also display different absorption spectra. They have been optimized in terms of water solubility, polarity, and cell-membrane permeability, and exhibit a pK_a value that enables the detection of small pH changes at around pH 7. The polar fluorescein derivative BCEFC (2′,7′-bis(2-carboxyethyl)-5-carboxyfluorescein; Figure 4) represents a typical dual-excitation ratiometric pH indicator,

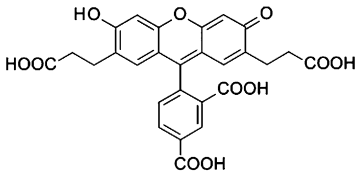

Figure 4. Chemical structure of the cell-permeable pH-sensitive probe BCEFC.

which is used for intracellular pH measurements.[14,15] The absorption maximum of the phenolate anion (basic form) undergoes a bathochromic shift with an increased absorption coefficient relative to the protonated (acidic) form. The probe is excited at 450 nm and 490 nm and the signal ratio acquired at a fixed emission window between 510 and 535 nm is calculated. A class of naphthofluorescein and seminaphthofluorescein derivates (SNARF and SNAFL)[15] have both dual-emission and dual-excitation properties and can be applied to cells, which makes them particulary useful for confocal laser-scanning microscopy and imaging, flow cytometry, and fiberoptic sensors.[16–18] FLIM can be carried out as an alternative to ratiometric 2-λ imaging.[19]

Sensor layers based on pH-sensitive probes can also be applied for the determination of CO_2[20] or ammonia[21] if water molecules are entrapped and a polymer matrix impermeable to ionic compounds and protons is used. Fluorescence sensors for CO_2 utilize the equilibrium that is formed between CO_2, water, and carbonic acid. Cross-sensitivity towards ionic strength can be minimized by using carboxyfluorescein ester derivatives as indicators.[22]

3.2. Oxygen- and Temperature-Sensitive Probes

Dynamic quenching of fluorescence represents a process that is frequently used in optical sensors. It is based on collisions between the excited fluorophore (donor) and the quenching molecule (acceptor). In 1935 Kautsky and Hirsch[23] described the decrease in the fluorescence and phosphorescence intensity of several organic dyes adsorbed on silica when exposed to oxygen. Depending on the donor–acceptor system, FRET or electron-exchange processes can account for nonradiative energy transfer from an excited state to a quencher.[24] The formation of charge-transfer (CT) states is another factor for the quenching mechanisms in the case of transition-metal complexes.[25] Nevertheless, it has to be kept in mind that Förster-type long-range dipole–dipole interactions require a spectral overlap of the electronic transitions of the donor and acceptor. Therefore, other mechanisms can play an important role, particularly in the case of triplet–triplet annihilation. In contrast to FRET, these are based on electron-exchange processes (Dexter excitation transfer)[26] and require a spatial overlap of the wavefunctions of the molecular orbitals of the donor and the acceptor. The donor is thereby transferred from a triplet to a singlet state (Figure 5).

The rate of energy transfer decreases exponentially with the distance between the donor and acceptor, and should not exceed 1 nm for an efficient transfer. Typical acceptors for dynamic fluorescence quenching which are also interesting targets for sensor devices are oxygen, heavy metal ions, and halide anions.

Demas et al.[27] have studied the quenching of luminescent transition-metal complexes of ruthenium(II), osmium(II), and iridium(III) by oxygen. It was found that CT excited states in transition-metal complexes can often be classified as mixed singlet–triplet spin–orbit states. They concluded from their data that the formation of singlet oxygen ($^1O_2$) is dominated by energy-transfer pathways. The luminescence

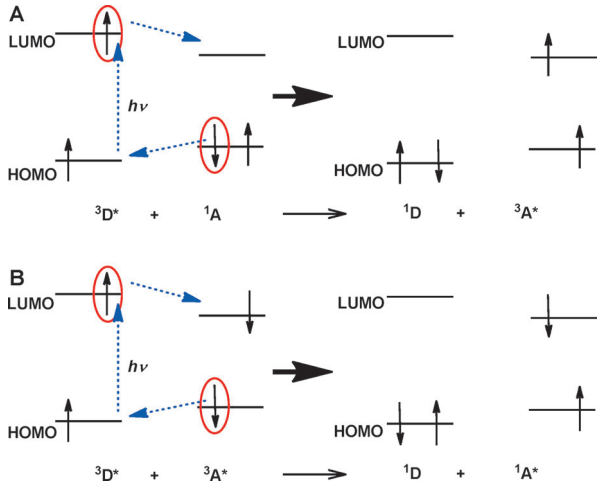

Figure 5. Electron exchange and energy transfer according to Dexter (top) and triplet–triplet annihilation between two excited triplet states (bottom) which yields two singlet molecules.

quenching mechanisms of ruthenium(II) complexes by heavy metal ions was characterized by Lin et al.[28] to be predominantly of electron-transfer nature. The main characteristic of dynamic quenching processes can be described by the Stern–Volmer Equation irrespective of the mechanism by which the excited state of the quencher is generated [Eq. (3)], where [Q]

$$\frac{I_0}{I} = \frac{\tau_0}{\tau} = 1 + K_{SV}[Q] \tag{3}$$

is the concentration of the quencher, K_{SV} the Stern–Volmer constant, and I_0 the luminescence intensity in the absence of the quencher. The Stern–Volmer constant is a measure of the quenching efficiency and determines the sensitivity of the probe to the respective quenching analyte. It is given by Equation (4), where k_q is the bimolecular quenching constant.

$$K_{SV} = \tau_0 k_q \tag{4}$$

It is clear that, in particular, triplet emitters with long-lived excited state lifetimes τ_0 can be quenched very efficiently.

Oxygen-sensitive phosphorescence probes have been reviewed extensively over the past few years.[29] Selected examples are summarized in Table 1 and Figure 6. Among the metalloporphyrins, which are favored indicators of oxygen because of their high brightness, palladium(II) and platinum(II) complexes of tetra(pentafluorophenyl)porphyrins (TPFPP) have found particular interest because of their high Stern–Volmer constants and photostabilities compared to the non-fluorinated meso-tetraphenylporphyrins and octaethylporphyrins.[30] Emission in the far-red and near-infrared (NIR) regions can be achieved with platinum and palladium porpholactons,[31] porphyrin ketones,[32] and benzoporphyrins.[33] Water-soluble probes for the determination of intracellular oxygen can be derived from coproporhyrins.[34] Other compounds used for oxygen sensing are ruthenium(III)[35] and iridium(III) complexes[36] as well as pyrene.[37] An exceptional fluorescent material which is quenched by small

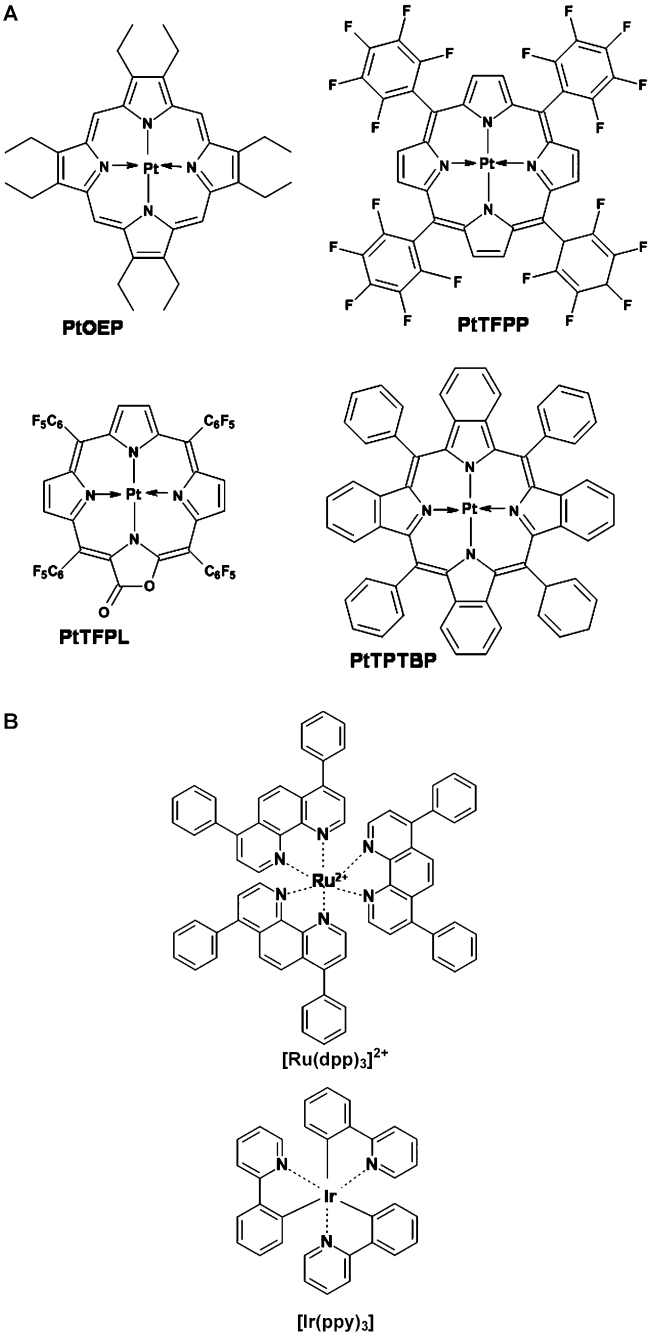

Figure 6. Examples of oxygen-sensitive luminescent metal–ligand complexes, whose spectral properties are described in Table 1.

amounts of oxygen is the fullerene C_{70}. Hence, dispersed in ethyl cellulose or organically modified silica (Ormosil), it can be used in sensors for trace amounts of oxygen.[38] The lifetimes listed in Table 1 are not absolutely comparable, as they are determined at different conditions and in different environments. Also the corresponding Stern–Volmer constants specified in the literature are not really comparable because of the different experimental conditions applied.

Thermal quenching is another phenomenon utilized in optical sensor technology. It exploits the decrease in photoluminescence intensity and lifetime with increasing temper-

Table 1: Photophysical properties of selected oxygen-sensitive probes

Probe	Absorption λ_{max} [nm]	Emission λ_{max} [nm]	Lifetime[a] τ_0 [μs] (matrix)	Ref.
$[Ru(dpp)_3]^{2+}$	450	600	5 (PS)	[39]
PtOEP	380, 535	647	90 (PS)	[40]
PdOEP	393, 512, 546	663	770 (toluene)	[41]
PtTFPP	395, 508, 541	650	55 (PS-PVP)	[30]
PdTFPP	406, 519, 552	660	910 (PS-PVP)	[30]
PtTFPL	392, 536, 575	735	45 (FIB)	[31b]
PtTPTBP	430, 564, 614	770	47 (toluene)	[33]
PdTPTBP	443, 578, 628	800	286 (toluene)	[33]
$[Ir(ppy)_3]$	375	512	1 (PS)	[36b]
$[Ir(btpy)_3]$	366, 408	596, 654	7 (polymer film)	[36b]

[a] At room temperature under exclusion of oxygen; [Ru(dpp)]: tris(4,7-diphenyl)-1,10-phenanthrolineruthenium(II); PtOEP: octaethylporphyrinplatinum(II); PdOEP: octaethylporphyrinpalladium(II); PdTFPP: meso-tetra(pentafluorophenyl)porphyrinpalladium(II); PtTFPP: meso-tetra(pentafluorophenyl)porphyrinplatinum(II); PdTPFPP: meso-tetra(pentafluorophenyl)porphyrinpalladium(II); PtTFPL: meso-tetra(pentafluorophenyl)porpholactoneplatinum(II); PtTPTBP: meso-tetraphenyltetrabenzoporphyrinplatinum(II); PdTPTBP: meso-tetraphenyltetrabenzoporphyrinpalladium(II); $[Ir(ppy)_3]$: tris-(2-phenylpyridine)iridium(III); $[Ir(btpy)_3]$: tris{2-(benzo[b]tiophene-2-yl)pyridinato-C^3,N}iridium(II).

ature. The Boltzmann distribution is one factor for this ubiquitous temperature effect, because it governs the population of the different vibrational levels of the electronic states involved. Temperature sensitivity occurs if two states of different nature are located within an energy difference of kT. Increasing the temperature influences the decay rates, emission intensities, and lifetimes because deactivating states are thermally activated. Nonradiative relaxation mechanisms, therefore, become dominant at higher temperature. The polymer used for the fabrication of sensor films also influences the temperature dependency because it can facilitate nonradiative relaxation of the excited luminophore by conversion into vibrational energy of the polymer matrix at higher temperatures.

Luminescent materials with high temperature coefficients are referred to as thermographic phosphors. These consist of inorganic ceramic compounds and are very robust in terms of their thermal stability. Typical examples are La_2O_2S and Y_2O_3 doped with Eu^{3+},[42] alexandrite,[43] sapphire,[44] and YAG (yttrium aluminium garnet) doped with Cr^{3+},[45] Tb^{3+}, or Dy^{3+}.[46] These cover broad temperature ranges from room temperature up to temperatures greater than 1000 °C. The photophysical principles of luminescence thermometry have been reviewed by *A*llison and Gillies.[47] Some europium(III) complexes with organic ligands also show a high temperature sensitivity, particularly with β-diketonates (Figure 7).[31b,48] The main temperature-dependent nonradiative relaxation mechanisms of the $^5D_0$ level of Eu^{III} chelates have been discussed by Berry et al.[49]

Certain ruthenium(III) and iridium(III) complexes are also suitable temperature-sensitive probes.[36b,50] Generally, the rate constants w of the crossover processes involved can be described by an Arrhenius-type equation [Eq. (5)], where

$$w = A \exp\left(\frac{-E_a}{kT}\right) \quad (5)$$

the barrier height is expressed by the activation energy E_a,[50] where A is the preexponential factor, k the Boltzmann constant, and T the absolute temperature. Accordingly, the lifetime τ of the emissive state can be expressed by [Eq. (6)], where k_0 is the

$$\frac{1}{\tau} = k_0 + k_1 \exp\left(-\frac{\Delta E}{RT}\right) \quad (6)$$

temperature-independent decay rate for the deactivation of the excited state, k_1 the preexponential factor, and ΔE the energy gap between the emitting state and the deactivating excited state.[51]

3.3. Probes for Metal Ions

Fluorescence indicators for metal ions such as Ca^{2+}, Mg^{2+}, Zn^{2+}, Na^+, and K^+ have found widespread application in clinical chemistry and bio-

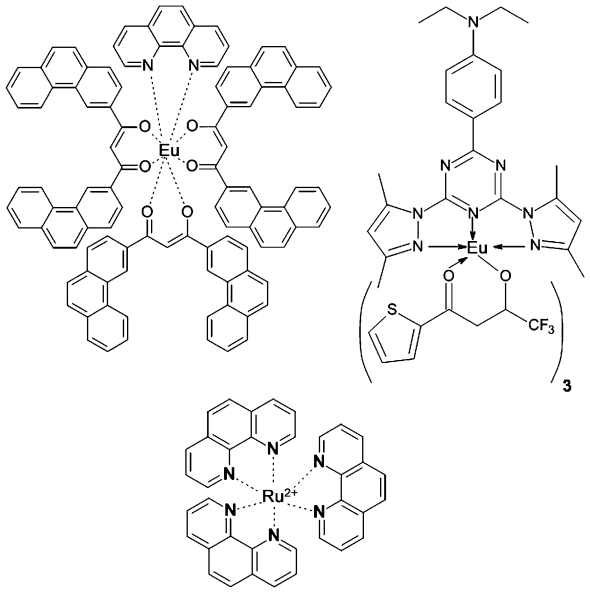

Figure 7. Temperature indicators used in optical sensors.

medical imaging. The imaging of the intracellular Ca^{2+} concentration and its distribution is an important tool in medical and pharmaceutical research. For example, the increase in cytosolic Ca^{2+} is a marker for the activation of pharmaceutically relevant cell-membrane-bound receptors and enzymes. Fluorescence probes are commercially available conjugated to dextrans for improved cellular retention or lipophilic dyes for studying near-membrane Ca^{2+} concentrations. The choice of proper cell loading and intracellular calibration methods are major tasks. The dissociation constant of the indicator–metal complex has to be compatible with the Ca^{2+} concentration range of interest. Ion indicators

exhibiting spectral shifts upon ion binding are suitable for ratiometric 2-λ methods. Among the numerous fluorescent calcium indicators, the class of fura dyes (e.g. fura-2)[52] with various dissociation constants for Ca^{2+} are prominent examples (Figure 8). These show a significant hypsochromic shift in

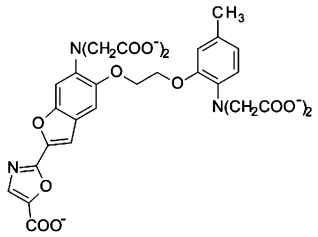

Figure 8. Chemical structure of the Ca^{2+}-sensitive probe fura-2.

the absorbance after binding to Ca^{2+} ions. The emission is typically monitored at 510 nm at dual excitation wavelenghts of 340 and 380 nm.[53] Alternatively, derivatives of Indo-1 may be used; this is a Ca^{2+}-sensitive dye with dual-emission properties ($\lambda_{em} = 400/470$ nm with/without Ca^{2+}).[54]

The drawback of these dyes is that they can only be excited with UV light. Therefore, several calcium-sensitive probes have been developed that can be excited with visible light, for example, Calcium Green-1 and 2[55] or the Oregon Green BAPTA dyes,[56] which are based on fluorescein or rhodamine derivatives.[57] These so-called fluoroionophores provide an improved selectivity as a result of the combination of a fluorophore with a specific recognition element (e.g. BAPTA; Figure 9). They respond with an increase in the fluorescence quantum yield upon calcium binding and are appropriate for the measurement of cytosolic calcium.

An intracellular indicator for Ca^{2+} which undergoes a high signal increase has been designed that bears two arsenic substituents on the fluorescein unit which bind selectively to tetracysteine-tagged proteins. This genetically targetable indicator enables localized measurements.[58] However, these fluorogenic probes have no capability for dual-wavelength measurements. Therefore, other ratiometric methods such as the addition of inert reference dyes or FLIM have to be applied. The same applies to other fluorescent metal-ion indicators, particularly for probes sensitive to Mg^{2+} (Magnesium Green),[59] Zn^{2+} (FluoZin-3), Cu^{2+} (Phen Green FL), and K^+ (PBFI).[60]

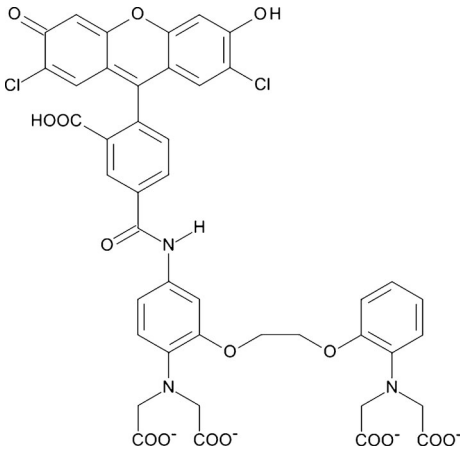

Figure 9. Calcium Green-1 consists of a dichlorofluorescein connected to the calcium-binding domain 1,2-bis(*o*-aminophenoxy)ethane-*N*,*N*,*N*′,*N*′-tetraacetic acid (BAPTA); $\lambda_{abs} = 505$ nm, $\lambda_{em} = 530$ nm.

Ratiometric 2-λ probes have been designed for cytosolic Na^+,[61] Zn^{2+},[62] and NH_4^+.[63] The biggest challenge for biomedical imaging will be the development of probes with improved selectivity for ions and excitation and emission wavelengths shifted to the red or NIR region.

Molecular probes based on photoinduced electron transfer (PET) are a valuable alternative to the metal indicators described above. In general, these molecules consist of a fluorophore, a spacer, and a receptor. The receptor bears free electron pairs, for example, on the nitrogen or oxygen atoms. One of these electrons can be transferred to the partially unoccupied HOMO of the photoexcited fluorophore. A back-electron transfer can now take place from the excited state of the fluorophore to the HOMO of the receptor. This leads to a radiationless deactivation of the excited state and the fluorescence is quenched. PET is blocked and the fluorescence of the molecule is turned on if a guest binds to the receptor (Figure 10). A quantitative approach to predict PET efficiency was developed by Weller.[64] PET is fast and fully reversible.

Intramolecular PET can occur over distances of 1–2 nm.[65] Typical receptor modules target for protons, metal

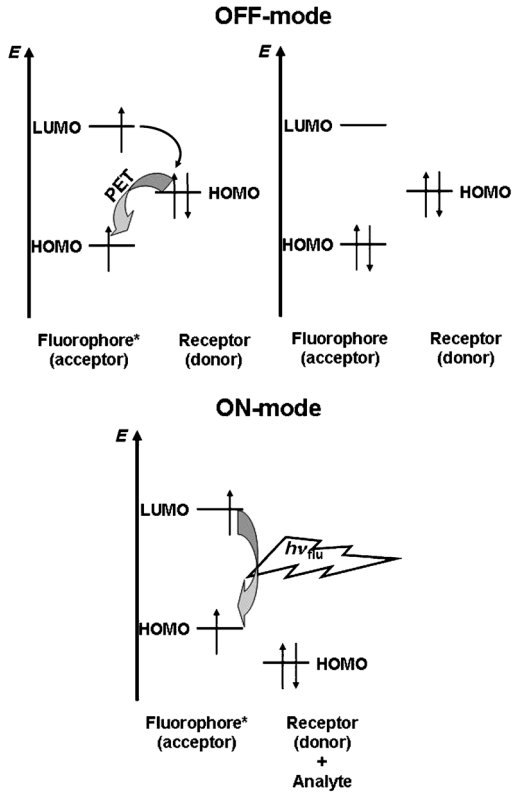

Figure 10. Simplified molecular orbital diagrams showing the relative energy arrangement of the HOMO/LUMO energy levels of the fluorophore and HOMO of the donor involved in PET. * symbolizes the excited fluorophore.

ions, glucose, or phosphates. Examples include amino groups for pH, crown ethers for sodium, and diamine tetraacetic acids for calcium sensing (Figure 11).[66] De Silva et al.[67]

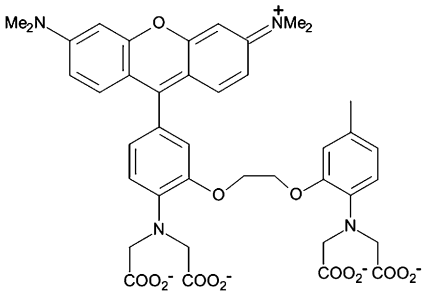

Figure 11. PET-controlled probe consisting of a fluorophore (rhodamine) that is quenched in the unbound state, a spacer, and a receptor (BAPTA) for recognition of Ca^{2+}.[66]

presented a variety of PET systems that can indicate host–guest recognition events and can also be employed as "molecular switches". A very useful fluoroionophore is composed of a naphthalimide fluorophore and aza[15]-crown-5 as a highly selective receptor for potassium.[68] Highly selective sensors for K^+ in aqueous solution can be obtained by incorporation in a polymer matrix and these, as well as other sensor elements, have found their way into commercialized optical blood gas and electrolyte analyzers.[69]

3.4. Lanthanide Complexes

Lanthanide complexes are a special case of molecular probes because they can be designed to respond to rather diverse analytes according to different sensing mechanisms. Complexes of the lanthanide ions europium(III) and terbium(III) are widely used luminescence probes and stains for biomolecular systems. Their applications were already discussed in 1982 in a pioneering review by Richardson.[70] Ligand coordination occurs predominantly through ionic interactions, thus leading to a strong preference for donor groups with negatively charged oxygen atoms (hard bases). Water molecules can also act as strong ligands for lanthanides and can be replaced by other hard donor groups, for example, hydrogen peroxide or phosphate anions. This reversible replacement makes lanthanide complexes promising luminescent probes applicable to chemical sensors. The complexation chemistry and ligand-exchange dynamics of lanthanide coordination chemistry have been reviewed by Parker et al.[71]

The luminescence spectra of Eu^{3+} complexes, which exhibit a $4f^6$ electronic configuration, are dominated by emission bands corresponding to the $^5D_0 \rightarrow {}^7F_J$ transitions. The strongest intensities are observed for $^5D_0 \rightarrow {}^7F_1$ and $^5D_0 \rightarrow {}^7F_2$ transitions. In particular, the latter one with its very strong and sharp emission line around 615 nm is the basis for the application of europium complexes as luminescence probes and labels.

The hypersensitivity of this transition is due to its electric dipole character, and the radiative transition probability is very sensitive to the nature of the ligand environment. The same is the case for the $^5D_4 \rightarrow {}^7F_5$ transition of Tb^{3+} ($4f^8$ electronic configuration) centered at 543 nm. Thus, the emission intensity responds to chemical (or biochemical) analytes that can interfere with these transitions.[72]

The direct electronic excitation of lanthanide ions is very inefficient because of their low absorption coefficients and the occurrence of nonradiative deactivation processes mediated by solvent molecules, particularly by water. Therefore, sensitizing ligands are applied. These sensitizers are often termed "antenna" chromophores. The use of antenna chromophores, such as acridone or diaryl ketones, result in the excitation wavelength for europium complexes, which is usually below 370 nm, being shifted to the visible region.[73]

In general, lanthanide complexes can be divided into two subgroups:[74]

The first comprises antennae that have a high coordination number and rigidity. These ligands contain macrocyclic or polydentate moieties that form chelate complexes with the lanthanide ion. Such ligands are often based on cyclen (Figure 12), cryptand, crown ether, or diethylenetriaminepentaacetic acid structures. These form polycyclic structures

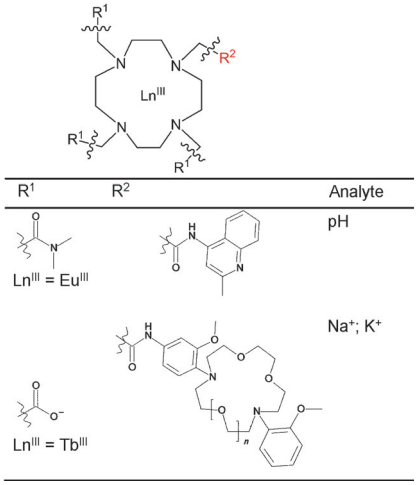

Figure 12. Cyclen-based lanthanide complexes as examples of ligand-based probes for pH value[76] or alkali metals.[78]

or polychelates with one or more lanthanide ions in combination with a molecular receptor or transition-metal complexes which can interact with the corresponding analyte.[75] Examples of molecular receptors combined with antenna systems include quinolines[76] and phenanthrolines[77] for pH-sensitive probes, crown ethers for the determination of Na^+ or K^+,[78] and chelators for heavy metal ions such as Zn^{2+}.[79] In other words, the luminescence of these kind of complexes is modulated by interactions of a chemical species with the sensitizing chromophore (ligand-centered process). Macrocyclic ligands can also be designed to encapsulate the lanthanide ion and protect it from interactions with the environment. These complexes provide a stable luminescence and can be used as labels and stains for biomolecular assays and biomedical imaging.[80]

The second group of lanthanide complexes includes ligands such as tetracycline derivatives (Figure 13) and fluoroquinolones that interact less strongly with the respective lanthanide ions. In these cases, the analyte acts as an

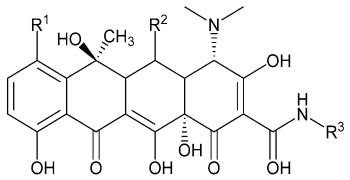

Figure 13. Tetracyclines as antenna chromophores for lanthanides. Tetracycline: $R^1 = R^2 = R^3 = H$; oxytetracycline: $R^1 = H$, $R^2 = OH$, $R^3 = H$; chlorotetracycline: $R^1 = Cl$, $R^2 = R^3 = H$.

additional ligand to the lanthanide center. Probes of the second type depend on an intermolecular energy transfer. Their luminescence is modulated by metal-centered interactions. The response occurs as a result of the exchange of additional ligands that are more or less strong quenchers. The overall structure of these complexes is often not determined and the best sensitivities are sometimes obtained by combining an odd ratio of lanthanide ion to ligand, usually with an excess of lanthanide ions. A large variety of lanthanide-based probes have been reported in the past few years that respond, for example, to hydrogen peroxide,[81] ATP,[82] GTP,[83] phosphate ions,[84] citrate,[85] proteins,[86] or DNA.[87] The complex formed from europium and tetracycline was incorporated into a polymer matrix to obtain reversible optical sensors for hydrogen peroxide which can be applied to FLIM.[81b] It was also found that hydrogen peroxide or ATP-sensitive probes can be used to monitor the activity of various enzymes.[88]

Applications of both types of lanthanide-based probes in chemical sensors have been reviewed recently.[89] Typical examples include optical sensors for oxygen, pH value, hydrogen peroxide, humidity, copper ions, and temperature. These types of lanthanide-based probes have some merits such as large shifts between the excitation and emission wavelengths and long luminescence lifetimes which make them suitable for time-resolved fluorimetry. Nevertheless, their lack of selectivity is a major drawback with respect to chemical sensing.

4. Sensor Nanoparticles for Chemical Imaging in Biological Systems

Spherical, nanometer-sized luminescent materials are frequently applied as biomolecular labels or in FRET assays. Their applications range from immunoassays to stains for in vivo imaging. The incorporation of dye molecules into rigid polymeric matrices paved the way for new biomolecular labels with superior brightness, photostability, and chemical stability. Furthermore, the fluorophores can be protected from quenching by oxygen or metal ions and are less affected by pH variations or other chemical interferences.[90] However, their implementation for the sensing of chemical species is only in its infancy.

4.1. Responsive Nanoprobes

Materials that are used most frequently for the preparation of polymeric nanoparticles (NPs) include silica, polystyrene, or derivatives of polyacrylic acid. These can be prepared with diameters lower than 100 nm with high monodispersity and equipped with sensoric functions. For this purpose, fluorescence probes are incorporated or attached to the surface of polymeric or silica NPs. Their utility can be enforced by using polymer matrices with analyte-selective permeability. Many organic polymers can be used for the fabrication of sensor NPs and loaded with various kinds of luminescence probes including nonpolar organic dyes[91] as well as polar phosphorescent metal–ligand complexes.[92] Fluorescent polystyrene NPs are commercially available in a wide variety of sizes and colors. The particles can be prepared by microemulsion polymerization and/or precipitation techniques and soaked with organic dyes or metal complexes according to the polarity of the material. The availability of materials covering the range from nonpolar (polystyrene) to polar and hydrophilic (polyacrylic acid and its derivatives) provides high flexibility in terms of the encapsulation of dyes and probes into materials for specific applications. Some polymeric materials are highly biocompatible and already used for in vivo applications.[93]

The encapsulation of fluorescence probes into nanometer-sized inorganic silica matrices can be carried out by a modified Stöber synthesis or by water-in-oil microemulsion techniques.[94] The dyes can be either physically incorporated or covalently bound to organically modified silanes such as 3-aminopropyltriethoxysilane or 3-mercaptopropyltrimethoxysilane.[95] It is not possible to dope silica with many common hydrophobic organic dyes or metal–organic complexes because of its hydrophilic nature. Nevertheless, examples can be found of ruthenium complexes.[96] A remedy is the use of organically modified silica (Ormosil) based on precursors such as phenyltrimethoxysilane, which incorporate hydrophobic dyes.[97] Alternatively, fluorophores can be coupled covalently to the particle surface by subsequent reaction with reactive surface functionalities. In this way, for example, complexing fluoroionophores for the determination of metal ions have been attached.[94b]

Nanosensors are mainly used to determine oxygen, pH value, and ions (e.g. Ca^{2+} and K^+) in biological matrices and cells, often in combination with imaging. These particles are sometimes termed PEBBLEs (probes encapsulated by biological localized embedding).[98] A luminescent indicator for oxygen [octaethylporphine ketone platinum(II)] and an inert reference were encapsulated in poly(decyl methacrylate) for the determination of dissolved oxygen in biological samples.[99] In a similar approach, PtOEP was incoporated into the shell of an Ormosil nanoparticle in combination with a reference dye to sense oxygen inside living cells.[100] The doping with internal reference dyes is an important prerequisite for sensor applications to enable ratiometric analysis. The analyte-sensitive luminescence of the probe can be referenced against a signal from a reference dye which is inert. An alternative referenced nanosensor for the imaging

of intracellular oxygen consists of PtTPFP as an indicator and a naphthalimide reference dye in polystyrene.[101]

The red fluorescent protein DsRed in polyacrylamide was used as the recognition element for copper ions.[102] A FRET-based sensor for the continous sensing of intracellular pH values was demonstrated by Peng et al. by incorporating the indicator bromothymol blue in a biocompatible polyurethane nanogel.[103] Intracellular calcium imaging can be carried out with derivatives of Indo-1 covalently attached to polystyrene microspheres.[104] The incorporation of 2′,7′-dichlorodihydrofluorescein diacetate in Ormosil nanoparticles leads to probes for the intracellular sensing of H_2O_2 with improved selectivity over other reactive oxygen species.[105] Recently, the NIR-emitting PdTPTBP was encapsulated in a polyacrylamide hydrogel that was conjugated to tumor-specific peptides for the determination of hypoxic conditions in cancer cells.[106] Ratiometric detection was accomplished by the co-loading of inert reference dyes such as Alexa 647. A referenced NIR nanoprobe based on PdTPTBP was applied to the in vivo imaging of tumor hypoxia in animal models.[107] The ultimate goal is to image these parameters not only inside living cells but also in vivo, for example, by means of animal fluorescence scanners.

4.2. Core–Shell Nanosensors

Core–shell systems represent a promising approach towards the construction of nanosensors. In particular, silicate and Ormosils with differing hydrophobic/hydrophilic properties are suitable materials. Interferences to the probe by the reference dye or FRET between the two dyes can be minimized by spatial separation of the reference and indicators. For example, the reference dyes can be encapsulated into cores with low analyte permeability, whereas the indicator dyes can be placed on the surface of the shell (Figure 14).

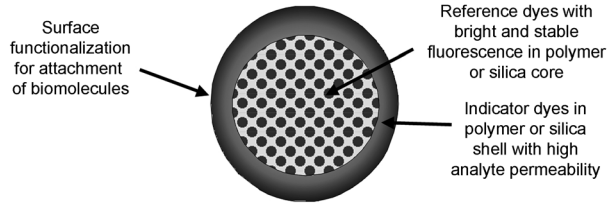

Figure 14. Schematic section of a core–shell nanosensor with an indicator and an inert reference dye.

Reference dyes may be conjugated to a silica core formed by condensation with 3-mercaptopropyltrimethoxysilane.[95b] Multifunctional silica particle systems can be tailored through this approach, which can combine sensor functions with other features, for example, magnetic properties (the so-called "C dots").[108]

The wrapping by a shell can also create a better biocompatibility and protein-repellent surfaces, for example, modified with dextran or poly(ethylene glycol),[109] and support the coupling of biomolecules. Silica shells can be used to coat various luminescent materials such as upconversion nanoparticles,[110] colloidal gold, silver, and QDs,[111] as well as organic polymer cores.[112]

In contrast, the high flexibility of the synthetic procedures also allow silica cores to be enclosed by polymer films, for example, by polystyrene.[113] Fluorescent core–shell particles based solely on organic polymers can be prepared from block copolymers with hydrophilic/hydrophobic units. Typical examples are poly(*tert*-butyl acrylate)-*block*-poly(2-hydroxyethyl methacrylate) functionalized with Texas Red[114] or poly(styrene)-*block*-poly(vinylpyrrolidone) loaded with a platinum porphyrin for oxygen sensing.[115]

5. Applications of Sensor Layers

In principle, luminescence probes and nanoparticles can be administered directly into biological matrices such as tissue to image the distribution, for example, of calcium,[116] magnesium,[59] pH value,[104,117] or hydrogen peroxide.[118] Genetically encoded probes based on conjugates with fluorescent proteins play an important role in in vivo imaging. A complementary approach consists of the use of sensor layers which are brought in contact to the sample. This avoids the contamination of the sample by dye molecules. However, this technique is restricted to 2D measurements. Analyte distributions can be imaged on surfaces, or profiles can be acquired along interfaces. These methods have found quite diverse application areas in biomedical imaging, such as dermatology and microbiology, as well as engineering. They enable the monitoring of physical and chemical parameters over relatively large areas and in real time. The state of the art of the so-called "sensor paints" was reviewed recently.[119] The following section is devoted to some outstanding examples of how these layers are applied in different fields of science and engineering.

5.1. Aerodynamics and Fluid Mechanics

The determination of the distribution of the absolute pressure on surfaces plays an important role in fluid mechanics and aerodynamic tests. The real-time imaging of dynamic flow processes on models in wind-tunnel tests is highly important for the aerospace and car industries. This led to the development of pressure-sensitive paints (PSPs). The function of PSPs is based on the principle of fluorescence quenching by oxygen. Peterson and Fitzgerald utilized the dynamic quenching effect of oxygen to study surface flows over silica-coated plates dyed with Fluorescent Yellow.[120] This led to the idea of PSPs. The first research on the application of PSPs to moving objects was performed at the Central Aero-hydrodynamic Institute (TsAGI) in Moscow in the mid 1980s. Since then, other aerodynamic research facilities worldwide have advanced the technique, including NASA (USA), JAXA (Japan), Onera (France), and the German Aerospace Center (DLR).

The concentration of oxygen in a sensor film is, according to Henry's law, proportional to the pO_2 above it in the case of

variations in the steady-state pressure.[121] PSPs consist of a mixture of indicator and polymer dissolved in an organic solvent and can be sprayed on various surfaces by using air guns to give uniform layers of several μm thickness (Figure 15). The requirements for the material are quite

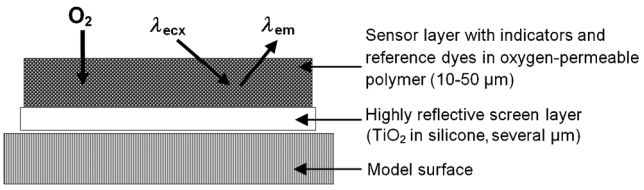

Figure 15. Schematic cross-section of a luminescent paint sensitive to air pressure.

high with respect to the homogeneity, evenness, mechanical stability, and photochemical stability of the incorporated dyes. The high costs of stainless-steel models for wind-tunnel tests necessitates that the paints should be removable after use without residues.

The addition of a reference dye improves the accuracy by compensating for interferences caused by light scatter, irregular illumination, and deformations of the model. Commonly used oxygen-sensitive probes for PSPs include pyrene as well as platinum and palladium-porphyrin derivatives.[121,122] A typical binary PSP formulation developed by DLR Göttingen in cooperation with the University of Hohenheim consists of a pyrene derivative as indicator and a europium complex as reference (Figure 16).[37] Another approach uses PtTFPL as the pressure-sensitive fluorophore and Mg^{II}-TFPP as the reference.[31a] The application of ratiometric luminescence lifetime imaging in combination with transition-metal complexes can circumvent the need for reference dyes.

The merit of PSPs compared to the use of single pressure taps is that the pressure distribution can be visualized with unsurpassed spatial resolution, even on parts of the model where pressure taps cannot be mounted. In principle, every pixel of the camera directed to the object acts as a sensor. The pressure distribution is acquired within several seconds, and flows on the surface can be visualized immediately. Turbulences and shock pulses can be identified. Lifting forces and bending moments can also be calculated from these data.

Technical aspects of PSPs are summarized in the monograph by Liu and Sullivan,[123] including specific techniques for measurement, image processing, and data analysis. In addition to wind-tunnel tests, in-flight PSP measurements can be conducted, for example, on fins, pylons, or wings of aircrafts, by using on-board cameras and excitation sources.[124]

The overall oxygen sensitivity exhibited by a luminescent sensor is basically predefined by the Stern–Volmer constant K_{SV}. According to the Stern–Volmer equation [Eq. (4)], fluorescence quenching by oxygen affects both the intensity and lifetime of the emission. While the natural lifetime τ_0 of a fluorophore is usually little affected by immobilization in a polymer matrix, the encapsulating polymer can cause

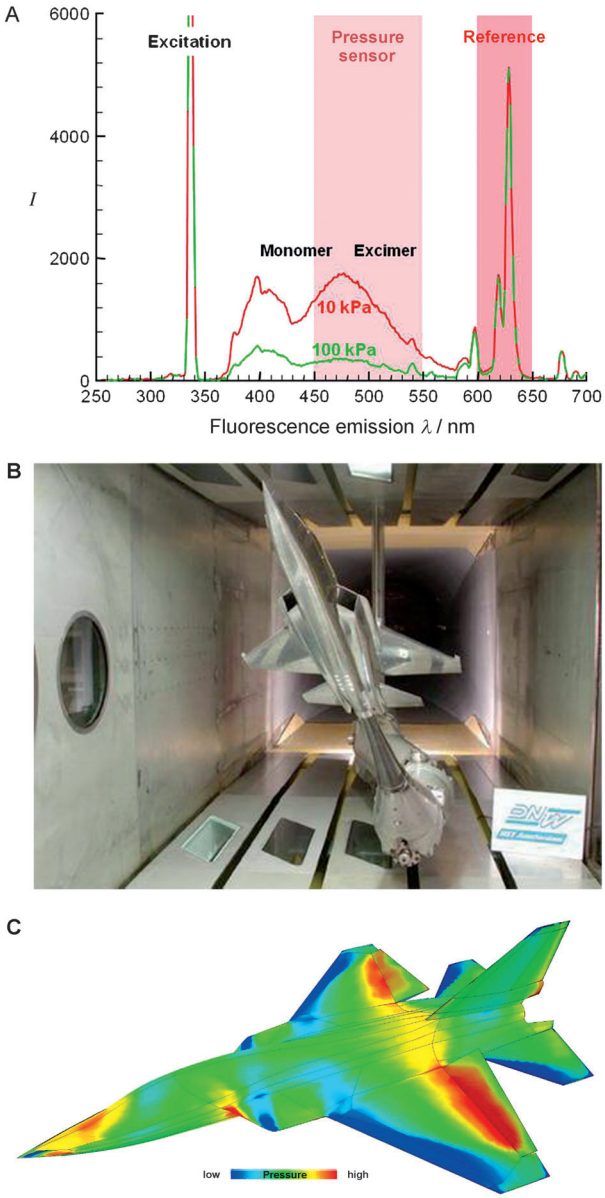

Figure 16. A) Emission spectra of a referenced PSP composed of pyrene and a europium complex dispersed in a polymer binder at different air pressures. The spectral ranges of the excitation light and the optical filters used for signal separation are also indicated. B) Model mounted in the test section of a wind tunnel. C) Image of the pressure distribution on a PSP-coated model. Reprinted from Ref. [37] with kind permission. Copyright (2005) Springer Science + Business Media.

a significant change in the sensitivity towards oxygen.[125] It is apparent that a high solubility and diffusion coefficient for oxygen in the polymer binder improves the oxygen sensitivity of the film. The transmission of gas molecules through polymer films is defined as the permeability. It can be quantified as permeability coefficient P, which is the product of the diffusion coefficient D and solubility coefficient S.

Accordingly, P can be defined as Equation (7), where $V =$

$$P = \frac{V(STP) \times d}{A \times t \times \Delta p} \qquad (7)$$

volume of gas (permeant), STP = standard temperature and pressure, d = film thickness, A = area, t = time, and Δp = pressure drop across film. Permeability varies greatly with temperature, according to an Arrhenius relationship.[126] Typical polymeric materials exhibiting high oxygen permeabilities include ethyl cellulose,[127] poly(dimethylsiloxane),[128] and poly(TMSP).[122] Fluoropolymers have a particularly high oxygen permeability as well as stability towards photooxidation and degradation by singlet oxygen. Common materials are FIB[129] and poly(IBM-*co*-TFEM).[122] The corresponding (co)monomer structures are summarized in Figure 17. Fast-responding oxygen-sensitive luminescent coatings for the imaging of unsteady pressure fluctuations have been deposited on surfaces of porous anodized aluminum.[130]

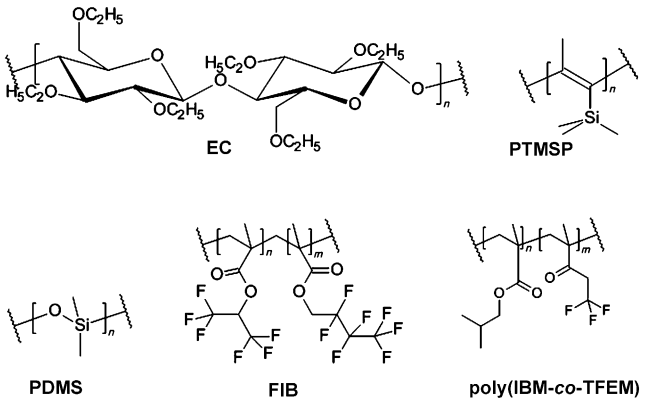

Figure 17. Polymer binders with high oxygen permeability used in PSPs. EC = ethyl cellulose, PTMSP = poly(trimethylsilylpropyne), PDMS = poly(dimethylsiloxane), FIB = poly(hexafluoroisopropyl methacrylate-*co*-heptafluoro-*n*-butyl methacrylate), poly(IBM-*co*-TFEM) = poly(isobutyl methacrylate-*co*-trifluorethyl methacrylate).

The deviation of dyes incorporated in polymer matrices from the linear Stern–Volmer relationship is often described by the "two-site" model according to Equation (8), with K^1_{SV} and K^2_{SV} being the two Stern–Volmer coefficients and f_1 and f_2 the corresponding emissive fractions.[35a] The multiple-site model can be attributed to the microheterogeneity of the luminophore environment leading to different accessibility of the quenchers. Nonlinear models for oxygen solubility and multisite models have been compared by Demas et al.[131]

$$\frac{I}{I_0} = \frac{\tau}{\tau_0} = \frac{f_1}{1 + K^1_{SV}[Q]} + \frac{f_2}{1 + K^2_{SV}[Q]} \quad (8)$$

There is also an urgent need in fluid mechanic research to visualize temperature gradients. The first substances used for this purpose were inorganic crystalline materials, which are known as thermographic phospors. Accordingly, the imaging of temperature distribution was termed "thermographic phosphor thermography". Recently, transition-metal and lanthanide complexes were used as luminescent indicators of temperature (Figure 7). By analogy to PSPs, they can be dispersed in polymer binders and are termed temperature-sensitive paints (TSPs). While these sensors are based on thermal fluorescence quenching, the thermally activated delayed fluorescence (TADF) of fullerene C_{70} displays an inverse effect. Dispersed in polystyrene (PS), it can be used as an optical sensor with an increasing delayed fluorescence at increasing temperature.[132] The TADF has a lifetime of approximately 20 ms and can be easily separated from the prompt fluorescence of an internal reference dye, such as perylene, by time-resolved fluorescence imaging.

Poly(acrylonitrile), poly(vinyl alcohol), poly(vinyl methyl ketone), and poly(vinyl chloride) are common polymer binders for TSPs. The critical issues in the selection of a polymer for a TSP are its thermal and mechanical stability as well as the photostability. The polymers that are used have very low oxygen permeability coefficients so as to avoid oxygen quenching. TSPs are mainly used for the study of hypersonic flows, heat transfer, transitions of laminar to turbulent flows (convection heat transfer is much higher in turbulent than in laminar flows), or shock pulses, particularly in cryogenic wind tunnels.[124,133] They also are applied in combustion studies in turbochargers and turbines. Temperature indicators are added to PSPs to compensate for the cross-sensitivity of oxygen-sensitive probes towards temperature. These materials will be highlighted in Section 6.

5.2. Biomedical Imaging

Since the pO_2 is significantly reduced in tumorous tissue,[134] the imaging of oxygen distribution by means of optical sensors is a useful tool in cancer research. NIR-emitting PdTPTBP modified with glutamate dendrimers was successfully applied to biological fluids and tumor cells in vivo.[135] Oxygen measurements were carried out by frequency-domain phosphorescence lifetime measurements. Zhang et al.[136] later used the red-emitting complex $[Ir(btp)_2(acac)]$ (acac = acetylacetanoate, btp = bis(2-(2′-benzothienyl)pyridinato-$N,C^{3'}$)) to image tumor hypoxia in vivo.

Alternatively, the supply of oxygen to malignant melanomas can be visualized with planar oxygen sensors. In this way, the efficacy of different protocols of photodynamic therapy can be evaluated on the basis of animal models.[137] Oxygen maps of an amelanotic melanoma prior and after photodynamic therapy were obtained by using a dorsal skinfold chamber attached to the back of a hamster. The images of the luminescence lifetime were generated by means of a CCD camera mounted onto an intravital microscope. The oxygen sensor layer consists of PtOEP in polystyrene. This transparent sensor allows the simultaneous visualization of the underlying microvasculature in the tissue.

The control of the oxygen supply is also of great interest in tissue engineering. Two-dimensional oxygen gradients were monitored with planar optodes consisting of PtOEP in silicone.[138] Numerous other quenchable probes have been applied in optical oxygen sensors, particularly perfluorinated porphyrins because of their improved photostabilities. Their compatibility with different polymer binders have been discussed by Amao.[41] The solubility of ionic dyes in apolar media can be improved by the exchange of hard counterions

by lipophilic organic ions. Another method consists of the covalent immobilization of the probe into the polymer network, for example, carboxyfluoresceins to amino-modified polymers, which prevents the indicators from leaching out into the sample.[139,140]

The study of wound-healing processes is an important issue in the field of dermatology. A biocompatibele 2D pH sensor was developed which is capable of imaging pH values over a wide proton concentration range for in vivo use.[141] Fluoresceinisothiocyanate bound to amino cellulose microparticles acts as the pH indicator and $[Ru(dpp)_3]$ in polyacrylonitrile microparticles as the internal reference. The particles were immobilized in a polyurethane hydrogel. The sensor was used in direct contact to the skin to image variations in the pH value during chronic cutaneous wound healing in humans (Figure 18). The sensor was illuminated with a 460 nm LED and the images were recorded with a time-gated CCD camera through a 530 nm long-pass filter.

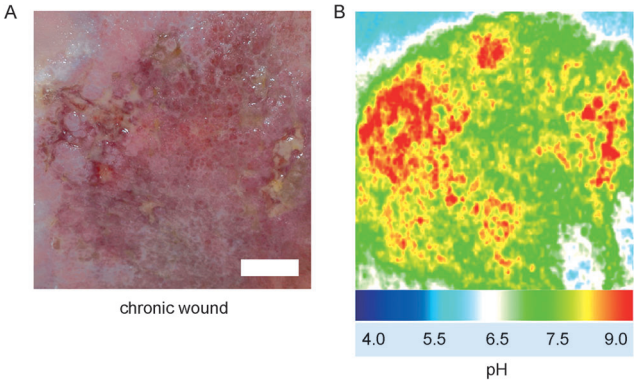

Figure 18. Luminescence imaging of pH value: Chronic venous ulcer (A) on the medial ankle of a human patient and the respective pH distribution as a pseudocolor image obtained with an optical sensor (B) shows an increased pH value in chronic wounds compared to the acid mantle of healthy skin. Scale bar: 1 cm. Reprinted from Ref. [141] with permission. Copyright (2011) National Academy of Sciences, USA.

5.3. Marine Microbiology

Planar optical sensors are useful tools in marine research, particularly in marine microbiology. The decrease in the pH value because of the global increase in atmospheric CO_2 is a major problem for calcifying organisms such as shellfish and corals at the sea bottom. The monitoring of seasonal changes of oxygen concentration and pH changes are further objects of analytical investigations. The dynamics of oxygen penetration into sediments[142] and oxygen consumption as a result of the degradation of organic matter can be monitored.[143] Furthermore, the bioirrigation activity, which is the active ventilation of animal burrows, of benthic macrofauna and its effect on the oxygen exchange between the sediment and the overlying water layer was studied by means of optical sensors.[144]

Microbiologists use oxygen sensors to determine the activity (respiration) of bacteria (oxygen-consuming or photosynthetically active bacteria) and microbial biofilms in sea sediments (Figure 19). Time-gated phosphorescence lifetime imaging is generally used to read out the planar optodes (Figure 2). These usually contain platinum or palladium porphyrins, for example PtOEP, in a polystyrene film and are particularly suited for measurements in oxygen-depleted environments.[145] Measurements can be performed in tanks as well as in the deep sea with a diver probe.[146]

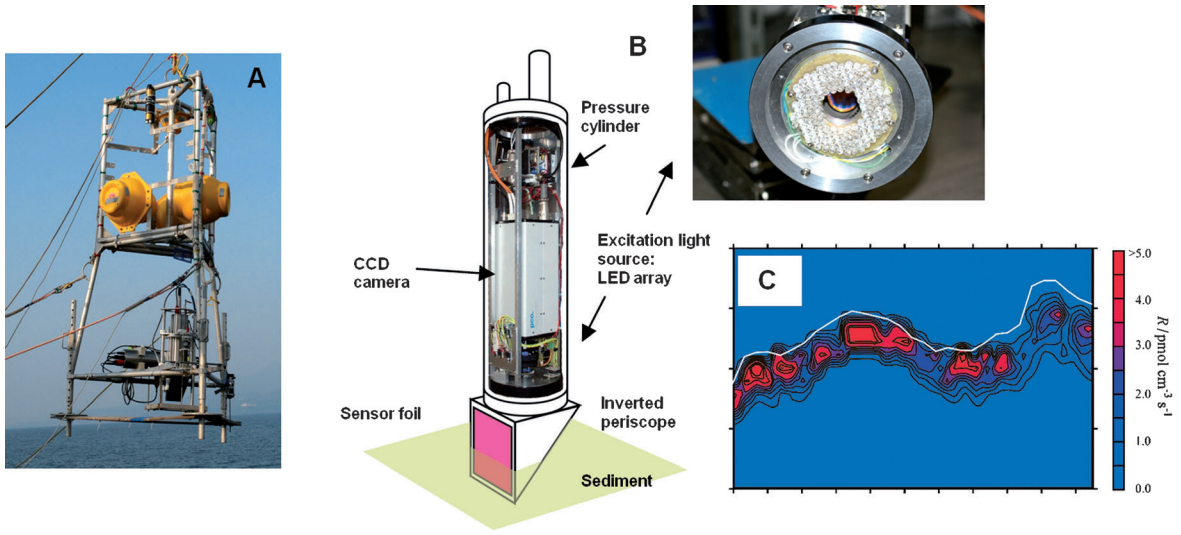

Figure 19. A) Lander system containing a fluorescence imaging system with a planar oxygen sensor for deap-sea measurements of oxygen profiles in marine sediments. B) Scheme of the sensor device (all photos courtesy of K. Oguri, JAMSTEC). C) Calculated 2D volume-specific O_2 consumption rate R from the O_2 distribution of a transect. The white line indicates the position of the sediment surface. Average oxygen penetration depth: 6.6 mm (Segami Bay, Japan, depth 1450 m). Reprinted from Ref. [146b] with permission. Copyright (2009) by the American Society of Limnology and Oceanography, Inc.

6. Multiple Sensors

Point-of-care analyzers including sensor arrays for the simultaneous determination of blood gases and electrolytes are the most prominent example of the use of optical sensors in the medical field. Instruments have been commercialized that contain disposable fluorescent sensor cartridges for the measurement of pH values, pCO_2, pO_2, Na^+, K^+, and Ca^{2+} in whole blood. These are based on different indicator molecules as described above.[4d,69] Additional cartridges are available for Cl^-, glucose, and urea and for the determination of total hemoglobin.

There are also several other motivations for the development of multiple sensors. One is to gather complementary information about a sample simultaneously, for example, the change of pO_2 and pH value in biological systems or the distribution of pressure and temperature on surfaces in fluid mechanics. The parallel detection of multiple parameters is also of great benefit in clinical chemistry as it reduces the time and increases the informative value of diagnostic findings. For example, the addition of glucose oxidase to an oxygen-sensitive layer led to a dual optical sensor for the simultaneous measurement of glucose and oxygen.[147] The application of multiple sensors that transmit different information from each reading point of the sensor layer is advantageous for imaging purposes. This possibility is a unique feature of luminescent sensors, as the optical signals can be separated spectrally or by time-resolved methods.

Almost all luminescent dyes are sensitive to temperature. Thus, the addition of temperature indicators is another important incentive for the development of dual or multiple sensors. The temperature channel can be used to adjust the temperature dependency of the other probe to obtain precise analytical data. The general design principles and spectroscopic methods for the interrogation of dual sensors have been reviewed by Stich et al.[29b] Dual (or multiple) optical sensing can be achieved by using multilayer sensors or single-layer sensors. The multilayer approach makes use of different indicators embedded in distinct polymer layers, and these are spread on a solid support. In single-layer sensors, the indicators are incorporated in one single polymer matrix. Their incorporation in appropriate polymer micro- or nanobeads turned out to be advantageous (Figure 20).

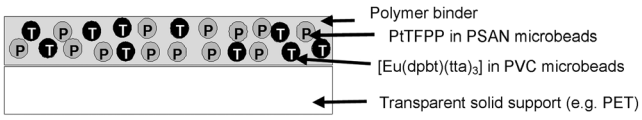

Figure 20. Cross-section of a dual sensor layer for imaging air pressure (*P*) and temperature (*T*).[148] PtTFPP and [Eu(dpbt)(tta)$_3$] serve as the indicators for oxygen (or *P*) and *T*, respectively. [Eu(dpbt)(tta)$_3$] = Eu(III)-tris(thenoyltrifluoroacetonato)-(2-(4-diethylamino-phenyl)-4,6-bis(3,5-dimethylpyrazol-1-yl)-1,3,5-triazine).

From a practical point of view, both luminescent probes in the sensor layer should be excitable by one light source. Thus, their absorption spectra have to overlap to a certain extent. The probes can be spatially separated from each other at a distance greater than the Förster radius by incorporation in different polymer micro- or nanoparticles. Furthermore, the sensitivity and selectivity of the indicators can be improved by the use of permeation-selective polymer beads. For example, poly(acrylonitrile) (PAN) is virtually impermeable to oxygen.[50b] Therefore, PAN microbeads can be used to shield temperature indicators from undesired oxygen quenching.

6.1. Dual Sensors for Oxygen and Temperature

The demand for dual PSPs/TSPs in aerodynamic research was a major driving force for the development of dual luminescent sensors. Large temperature gradients on the surface of a model can occur in high-speed wind-tunnel experiments. This effect has to be compensated for if the pressure distribution is to be imaged, as most oxygen-sensitive probes are prone to thermal quenching. The first approach was demonstrated by Coyle and Gouterman.[42] They used PtTFPP in FIB polymer for the lifetime imaging of pressure,

Table 2: Materials for dual sensing of oxygen (or air pressure) and temperature.[a]

Oxygen indicator	Temperature indicator	Polymer matrix	Ref.
PtTPFP	$La_2O_2S:Eu^{3+}$	FIB	[42]
$[Ru(dpp)_3]^{2+}$	MFG	Ormosil	[152]
PtTFPP	$[Ru(phen)_3]^{2+}$	PtBS-*co*-TFEM	[153]
PdTFPP	$[Ru(phen)_3]^{2+}$	polyurethane	[154]
in PSAN particles	in PAN particles		
PdTFPP	Eu-β-diketonate complexes	polyurethane	[155]
in PSAN particles	in PtBS particles		
PtTFPP	[Eu(dpbt)(tta)$_3$]	polyurethane	[156]
in PSAN particles	In PVC particles		
C_{70}	$[Ru(phen)_3]^{2+}$	ethyl cellulose/PAN two-layer system	[157]
$[Ir(btpy)_3]$	[Ir(carbaz)(ppy)$_2$] in PAN particles	cellulose acetate butyrate	[151]
PtTFPP in PS-*co*-PVP	[Ir(carbaz)(ppy)$_2$] in PAN particles	dispersion in water	[115]

[a] Carbaz:1-(9*H*-carbazol-9-yl)-5,5-dimethylhexane-2,4-dione; phen: 1,10-phenanthroline; MFG: manganese-activated magnesium fluorogermanate; ptBS-*co*-TFEM: poly(4-*tert*-butylstyrene-*co*- 2,2,2-trifluoroethyl methacrylate); PSAN: poly(styrene-*co*-acrylonitrile); PtBS: poly(4-*tert*-butylstyrene); PS-co-PVP: poly(styrene-*co*-vinylpyrrolidone).

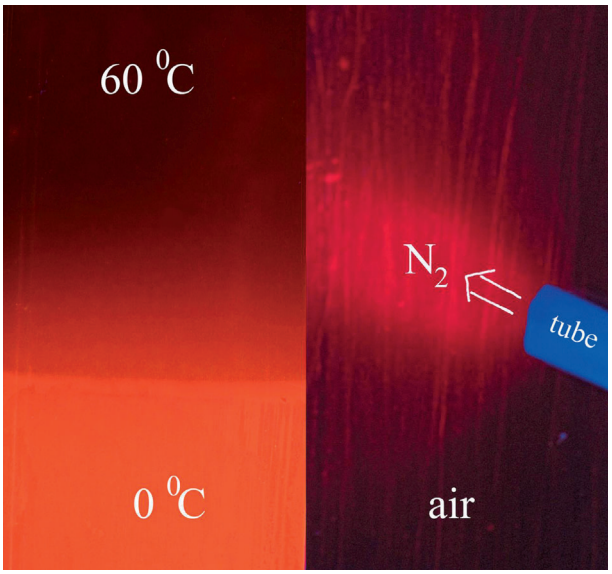

Figure 21. Luminescence images of a dual sensor foil ($[Ru(phen)_3]^{2+}$/PdTFPP). Left: temperature gradient imaged through a 580 nm bandpass filter. Right: oxygen partial pressure for the same sensor foil imaged through a 650 nm longpass filter at an excitation wavelength of 366 nm. Reprinted from Ref. [154] with permission.

and added particles of the thermographic phosphor $La_2O_2S:Eu^{3+}$ for the correction of the temperature dependency of the PSP. A series of different compositions were developed in the following years. These are summarized in Table 2. The thermographic phosphors were subsequently replaced by metal–ligand complexes. The two sensor outputs can be spectrally separated by changing the optical filters (Figure 21) if the two probes are selected properly according to their emission maxima.

New perspectives arise from the implementation of cyclometalated iridium(III) complexes bearing ligands derived from 2-phenylpyridine (ppy) or mixed ligand systems containing acetylacetonate groups. A large number of these phosphorescent triplet emitters with a variety of structures have been synthesized for use in organic light-emitting diodes (OLEDs).[149] They are available with different emission colors that cover the whole visible spectral range and show broad absorption bands in the blue region. However, only a few of these cyclometalated complexes are sensitive to oxygen quenching and can be used for oxygen sensing.[36,150] In general, the phosphorescence of these iridium complexes is not greatly affected by temperature, but the finding that the mixed ligand complex $[Ir(carbaz)(ppy)_2]$ shows a high temperature sensitivity paved the way for dual one-layer pO_2/T sensors based solely on iridium complexes.[151] In this approach, the complex $[Ir(btpy)_3]$ is used as the oxygen-sensitive probe. It shows a viable K_{SV} value and a very broad dynamic range which is superior to established oxygen probes, such as PtTFPP.

Dual sensors for the simultaneous determination of temperature and oxygen are not only required for aerodynamic research, there are also in demand for (bio)chemical process control, in medical research and diagnosis, and in microbiology.

6.2. Dual Sensors for Oxygen and pH Value

The first approaches towards dual sensors for oxygen and pH value consisted of two-layer systems. In a pioneering study, the pH indicator HPTS was used for CO_2 monitoring. It was covalently bound to cellulose particles dispersed in a hydrogel matrix. The oxygen-sensitive layer was composed of $[Ru(2,2'\text{-bipy})_3]^{2+}$ (2,2′-bipy = (2,2′-bipypyridyl) adsorbed on silica microparticles in silicone.[156] Response times of up to five minutes for the sensing of the pH value or for CO_2 have been significantly reduced now and are typically in the range of $t_{90} = 90$–120 s. One decade later, Klimant et al.[39] improved this approach by incorporating HPTS in ethyl cellulose particles. These were dispersed in PDMS and cast over an oxygen-sensitive bottom layer of PtTFPP in polystyrene. It took nearly another ten years until Borisov et al.[157] developed this work further by incorporating HPTS as a lipophilic ion pair with a tetraoctylammonium (TOA) cation in micrometer-sized ethyl cellulose beads. These were homogeneously dispersed in a highly gas-permeable silicone rubber. Additionally, inert reference beads containing an iridium(III) coumarin complex were blended. Again, the subjacent oxygen-sensitive layer consisted of PtTFPP in polystyrene.

The fabrication of single-layer sensors is preferred for imaging applications, but is generally very difficult to achieve from a materials perspective. Oxygen sensors require materials that are highly gas permeable but impermeable to ions and protons. In the case of pH sensors, the opposite is desirable. The first solution to this problem[158] again makes use of two different permeation-selective microbeads for the sensing of pH changes (carboxyfluorescein covalently attached to amino-modified *p*-HEMA) and oxygen ($[Ru(dpp)_3]^{2+}$ in Ormosil). Both were dispersed in a polyurethane hydrogel. The dual sensor can be used to monitor bacterial respiration and cell growth. In a similar approach, carboxyfluorescein was replaced by HPTS to enable the monitoring of bacterial growth.[159] In a further step towards improved one-layer sensors the lipophilic ion pairs HPTS/TOA and $[Ru(dpp)_3]$/TMS (TMS = trimethylsilylpropanesulfonate) were dissolved directly in ethyl cellulose. The resulting sensor was used for the time-resolved imaging of pCO_2 and pO_2 in aquatic environments.[160] The lipophilic pH-sensitive fluorescein derivative DHFA (2′,7′-dihexyl-5(6)-*N*-octadecylcarboxamidofluorescein) and PtTFPP can also be directly dispersed into a hydrogel matrix polymer. Gradients of pCO_2 and pO_2 can be mapped by using these 2D sensor layers at the boundary layer between seawater and marine sediments.[161] Recently, a sensor layer for the in vivo imaging of oxygen and pH value on skin was presented, which utilized PtTFPP and fluoresceine isothiocyanate conjugated to amino cellulose as the corresponding probes in a polyurethane film.[162] Diphenylanthracene dispersed in PAN microparticles was added as the reference fluorophore. The three channels of the sensor can be read out by means of digital RGB color cameras.

6.3. Dual Sensors for pH Value and Temperature

Only a few examples for the simultaneous sensing of pH values and temperature are described in the literature. As outlined above, many suitable fluorescent pH indicators are 2-λ probes with two different broad absorption/emission bands for the protonated and deprotonated form, thus covering a substantial range of the visible spectrum. This makes the spectral separation of the emission of a second dye rather difficult. Europium(III)-β-diketonates have a narrow emission band in the red region of the spectrum and show a very high temperature sensitivity. Hence, the complex $[Eu(tta)_3(dpbt)]$ was used for the first dual pH/*T* sensor in combination with HPTS as a pH indicator.[163] A recent approach makes use of a thermographic phosphor (chromium(III)-activated yttrium aluminum borate) as an intrinsic temperature control of a pH sensor based on a SNARF derivative.[164] Both dyes can be excited by a red 605 nm LED and emit in the NIR. The combination of a fast-decaying pH indicator and a phosphorescent temperature indicator was interrogated by means of the dual lifetime referencing (DLR) method (see Figure 23 in Section 7). Furthermore, colorimetric pH/*T* sensors have been developed by combining a pH-responsive solvatochromic dye with a thermoresponsive polymer.[165]

An assembly of two dual sensors in two stacked layers was developed to monitor oxygen, carbon dioxide, pH value, and temperature.[166] The lower layer comprises indicators for O_2 (an Ir^{III} complex in polymer microbeads) and CO_2 (HPTS) in ethyl cellulose, and the upper layer indicators for temperature (microcrystalline chromium(III)-doped yttrium aluminum borate phosphors) and pH value (SNARF-DE) in polyurethane. Both sensor components have to be excited with different wavelengths (450 nm and 605 nm). The necessity for two separate excitation sources makes this set up less practicable for imaging applications, but it is interesting for fiberoptic sensors.

6.4. Triple Sensors

The idea of using separable emission wavelengths of different fluorescent indicators for the fabrication of triple sensors was formulated for the first time in 1988 by Wolfbeis et al.[156] Triple sensor in this regard means that three sets of information can be obtained from one sensor spot. Of course, sensor arrays with three discrete sensors were developed earlier, for example optical fiber arrays for blood gas analysis.[167] However, the triple sensor material approach is much more favorable for imaging applications. Astonishingly, it took over 20 years until this concept was realized. For the first optical triple sensor, pH-, oxygen-, and temperature-sensitive probes were incorporated into different polymer microbeads and dispersed in a polyurethane layer (Figure 22).[168] The sensor read out is performed by a combination of spectral separation and time-resolved luminescence detection (RLD), from which the emission of the long-decaying temperature indicator $[Eu(dpbt)(tta)_3]$ can be isolated.

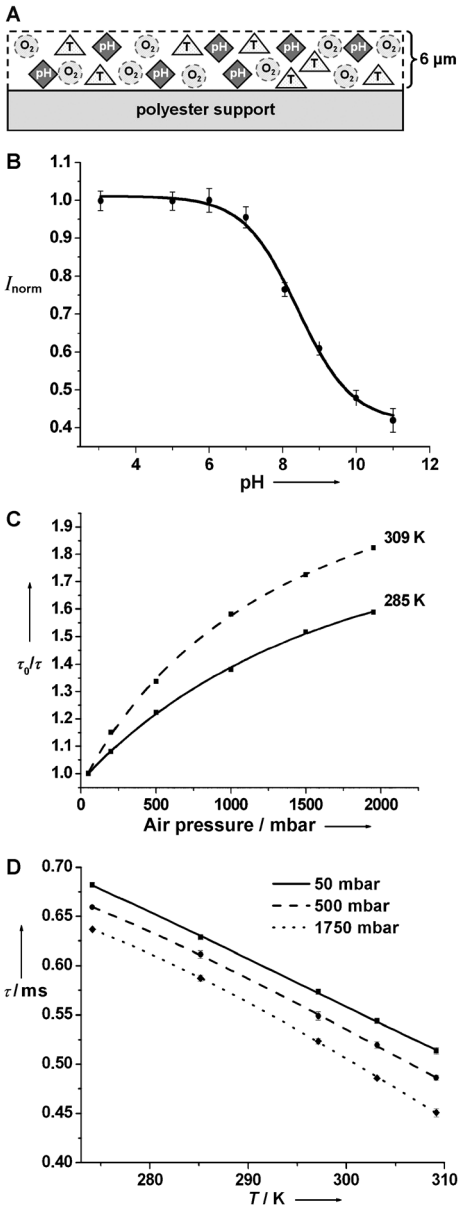

Figure 22. A) Cross-section of a triple sensor which consists of a polyurethane hydrogel with three kinds of luminescent beads: (◇) pH-sensitive beads (HPTS in pHEMA), (△) temperature-sensitive beads ($[Eu(dpbt)(tta)_3]$ in PVC), and (○) pO_2-sensitive beads (PtTFPP in PSAN). Response of the sensor to B) pH, C) O_2 at different temperatures, and D) temperature. Reprinted from Ref. [170].

7. Signal Interrogation

The interrogation of multiple sensors requires advanced imaging techniques. It is difficult to achieve a full spectral resolution if more than two probes are applied, because spectral overlap can usually not be avoided. Consequently, techniques with a temporal resolution have to be combined, namely time-gated fluorescence detection is needed. These pulsed methods are a valuable complement if the separation achieved by optical filters is not sufficient. A simple way to separate the luminescence of a long-lived indicator from crosstalk of a second short-lived dye is to image the intensity

of the long-lived indicator within a time gate that is positioned after the fluorescence of the short-lived component has decayed (time-resolved fluorescence). The use of the RLD method (see Figure 2) is even more sophisticated. In this case, the change in the luminescence lifetime τ of the long-lived probe can be employed as intrinsically referenced information. For example, portable optical sensor devices for oxygen are based either on time-resolved pulsed fluorescence detection, by using, for example, PtOEP in PS as a sensor layer,[169] or on frequency-domain measurements (PtOEP in Ormosil).[97]

The time-domain dual lifetime referencing (td-DLR) method[140] makes use of a short-lived fluorescent indicator combined with a long-lived phosphorescent reference dye. (Figure 23 A). It is based on the acquisition of two images, one

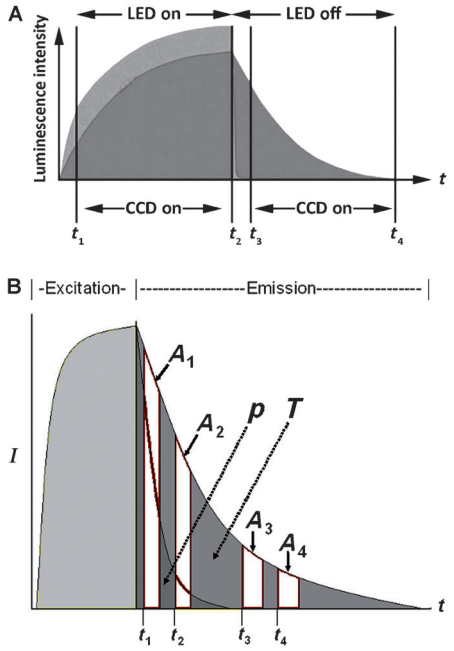

Figure 23. A) Scheme of the td-DLR method that enables the referencing of a fluorescence sensor with a long-lived reference dye. I_{Ex}: Image acquired during excitation phase; I_{Em}: Image acquired during emission phase (intervals with CCD on). B) Scheme of the DLD method that calculates the average lifetime of two components, in the first two gates (*A*1, *A*2) a mixed lifetime of both indicators, and in the second two gates (*A*3, *A*4) the pure lifetime of the longer-lived indicator (e.g. a temperature indicator). The contribution of the short-lived indicator, for example, for air pressure, can be calculated from these data.

taken in the excitation period (I_{Ex}) and one in the emission period (I_{Em}) after the pulsed light source has been turned off. The intensity I_{Ex} represents the sum of the short-lived indicator and the long-lived phosphorescence of the reference, while I_{Em} originates exclusively from the reference. Again, interferences can be referenced out by dividing I_{Ex} by I_{Em}. Recently, td-DLR was used for the in vivo imaging of pH gradients during cutaneous wound healing (Figure 18).[141] DLR is also a valuable referencing scheme for frequency-domain measurements (fd-DLR).[157]

The dual lifetime determination (DLD) approach requires the acquisition of four time-gated images. It is applicable if the luminescence decay time of a long-lived probe is at least about 10 times longer than that of the short-lived component. The lifetime image calculated by the division of A_3 by A_4 contains exclusively the information on the long-lived part (τ_2) of the sensor. The ratio calculated from A_1 and A_2 reflects the mixed decay of both luminophores (Figure 23 B). The fraction of the fast-decaying component τ_1 can be calculated by iterative data evaluation processes or three-dimensional calibration functions. This method provides lifetime data for both indicators and can be used, for example, for the read out of a dual PSP/TSP[148] or for monitoring the oxygen consumption of enzymatic reactions with simultaneous control of the temperature.[170] The latter example paves the way for triple sensors that can monitor glucose, oxygen, and temperature.

Other techniques for the identification of multiplexed lifetime signals apply pattern-matching algorithms[171] or assume that the mixed decay curve behaves as a linear combination of the decay functions of the single components.[172] The analysis requires time-correlated single-photon counting to record the whole decay curve from which the contributions of the single fluorophores can be calculated by decay-pattern recognition. Nevertheless, photon counting methods are currently too complex and expensive to be used in praxis for sensing or imaging.

Recently, it was demonstrated that the fluorescence signals of different indicators can be separated by means of RGB-sensitive pixels of CMOS (complementary metal oxide semiconductor) chips in inexpensive digital color cameras.[163] The aim is to integrate into the sensor appropriate indicators whose fluorescence emissions match the sensitive wavelength ranges of the RGB pixels. In this basic approach, the pH indicator HPTS was used for CO_2 (blue channel) and [Eu(dpbt)(tta)$_3$] for temperature (red channel) imaging. The two channels can be analyzed quantitatively with the help of a commonly used image-processing software. This concept was modified and improved by the incorporation of an inert dye to obtain an intrinsic referenced oxygen sensor by using the red (oxygen) and green (reference) channel of the RGB chip.[173] Oxygen levels can be imaged with high precision by dividing the signal intensities of the red and the green channel. This approach represents a versatile detection method, as colorimetric assays can also be read. This was demonstrated by means of sensor arrays for pH values and metal ions[174] or biogenic amines.[39]

8. Conclusion and Outlook

This Review considers the field of chemical fluorescence imaging with respect to probe design and functionality, referencing, sensor materials, and signal processing. For a more detailed discussion on the theoretical background of fluorescence sensing the reader is referred to the books by Valeur,[175] Lakowicz,[176] and Demchenko.[177] The development of appropriate sensor materials and read-out techniques is a highly interdisciplinary challenge. It combines synthetic

organic and inorganic chemistry, material science, (time-resolved) fluorescence spectroscopy and imaging, methods for signal separation, computing, and engineering.

In fact, only a small selection of all the luminescence probes described in the literature has made its way into optical sensors. The huge variety of probes that have been developed for other analytes, such as carbohydrates,[178] hydrogen peroxide,[179] ATP,[180] and anions,[181] are not considered because they have not been utilized up to now in sensor layers for imaging applications. The lack of reversibility, photostability, chemical stability, and selectivity in real samples, in general, represent major obstacles. Nevertheless, optical sensors have distinct advantages compared to electrochemical sensors, because of the fact that light propagates through air and transparent matter. Thus, remote sensors can be designed with the sensor layer placed inside (bio)reactors, small samples, interfaces, microfluidic systems, cells, biological tissue, or domains which are difficult to access. An unsurpassed density of sensor spots is available in combination with imaging methods, which is only limited by the number of pixels of the camera used for detection and leads to microscopic resolution. Applications include process control, fluid mechanics, medical imaging, pharmaceutical screening, and microbiology. NIR probes are becoming more and more important. In particular, NIR fluorophores that change their fluorescence upon a specific reaction with biologically active molecules are of great interest for medical research and diagnosis, as well as for in vivo imaging.[182]

The significance of imaging parameters such as pH value, pO_2, H_2O_2, and Ca^{2+} in medicine has been outlined, for example, in cancer research, transplantation medicine, tissue engineering, and for the study of wound-healing processes. Except for sensors for pH value, pO_2, and some ions, the reversibility and selectivity of the recognition system to enable continuous monitoring of other analytes is a major challenge for a further improvement and application of optical sensors. In particular, there is a lack of reversible and specific probes for H_2O_2, biophosphates such as ATP, and glucose, just to name a few. Biocompatible probes for the imaging of temperature also show great potential, for example, to monitor thermal therapies (hyperthermal treatment) for cancer. New materials such as as fluorescence upconversion nanocrystals show great potential for sensing applications in biological samples, as they can be excited in the NIR (980 nm) and show an anti-Stokes' shift. The different emission bands in the visible spectrum, for example, of $NaYF_4$ doped with Yb^{3+} and Er^{3+}, can be used to determine the temperature inside cells or tissue by means of ratiometric imaging.[183]

In some applications the response should not only be reversible, but also very fast. This is particularly necessary for unsteady measurements, for example, for unsteady PSPs which have to indicate dynamic pressure changes on moving or rotating elements with millisecond resolution. This is a challenge for the design of the probe and the matrix polymer, which needs to have a high permeability for oxygen, as well as for signal recording.

Sensor nanoparticles will have an increasing importance in biomedical imaging. Probes whose surfaces are functionalized with biomolecules, such as antibodies or peptides, can be targeted to cancer cells to monitor relevant parameters in cancer research and therapy (e,g. pO_2, pH value, or certain signaling molecules). Modification of the surface of nanoparticles can also reduce their cytotoxicity, facilitate their internalization into cells, and extend their circulation time in the bloodstream. The last factor is required to enable the nanoprobes to reach their target cells. This is achieved with protein-repellent surfaces, such as PEG or dextrans.

Scientific CCD cameras are usually applied in fluorescence imaging. The progress of CMOS-based detector arrays and digital cameras enable the application of more cost effective and compact devices. Furthermore, chemical sensing and imaging with familiar, mass-produced devices, such as computer screens and web cameras,[184] flatbed scanners,[185] mobile phone displays and cameras,[186] and digital color cameras,[163] opens up new perspectives for the dissemination of these techniques. The last approach is particularly useful for multiple sensors if the luminescence emissions of the probes can be adjusted to the maximum sensitivity of the RGB channels or pixels of the camera. From a materials perspective, the utilization of polyelectrolyte multilayers or the combination of fluorescent receptors with molecularly imprinted polymers could lead to optical sensor materials with improved selectivity and reversibility.

I gratefully acknowledge Dr. Ulrich Henne, Dr. Christian Klein, Dr. Kazumasa Oguri, Dr. Matthias Stich, Dr. Robert Meier, and Lorenz Fischer for providing the photos and graphics, as well as Prof. Otto S. Wolfbeis and also the German Aerospace Center (DLR) Göttingen for financial support.

Received: August 2, 2011
Revised: October 12, 2011
Published online: March 15, 2012

[1] a) *Biomedical Photonic Handbook* (Ed.: T. Vo-Dinh), CRC, Boca Raton, **2003**; b) B. Herman, Fluorescence Microscopy, 2nd ed., Taylor & Francis, New York, **1998**; c) J. W. Lichtman, J.-A. Conchello, *Nat. Methods* **2005**, *2*, 910 – 919.

[2] D. R. Thevenot, K. Tóth, R. A. Durst, G. S. Wilson, *Pure Appl. Chem.* **1999**, *71*, 2333 – 2348.

[3] "The Cambridge Definition of Chemical Sensors": K. Cammann, E. A. Guibault, H. Hall, R. Kellner, O. S. Wolfbeis in *Proceedings of the Cambridge Workshop on Chemical Sensors and Biosensors*, Cambridge University Press, New York, **1996**.

[4] a) O. S. Wolfbeis, *Anal. Chem.* **2006**, *78*, 3859 – 3874; b) S. Arain, G. T. John, C. Krause, J. Gerlach, O. S. Wolfbeis, I. Klimant, *Sens. Actuators B* **2006**, *113*, 639 – 648; c) J. K. Tusa, H. He, *J. Mater. Chem.* **2005**, *15*, 2640 – 2647.

[5] For example, the "Opti CCA Blood Gas and Electrolyte Analyzer" from Opti Medical Systems.

[6] a) G. Gauglitz, *Anal. Bioanal. Chem.* **2005**, *381*, 141 – 155; b) O. S. Wolfbeis, *Anal. Chem.* **2008**, *80*, 4269 – 4283; c) S. Nagl, O. S. Wolfbeis, *Analyst* **2007**, *132*, 507 – 511; d) C. McDonagh, C. S. Burke, B. D. MacCraith, *Chem. Rev.* **2008**, *108*, 400 – 422.

[7] "Intrinsically Referenced Fluorimetric Sensing and Detection Schemes: Methods, Advantages and Applications": M. Schäferling, A. Duerkop in *Standardization and Quality Assurance in Fluorescence Measurements I, Springer Series on Fluores-*

cence, *Vol. 5* (Ed.: U. Resch-Genger), Springer, Berlin, **2008**, pp. 373 – 414.

[8] a) S. B. Bambot, J. R. Lakowicz, G. Rao, *Trends Biotechnol.* **1995**, *13*, 106 – 115; b) M. Y. Berezin, S. Achilefu, *Chem. Rev.* **2010**, *110*, 2641 – 2684.

[9] R. J. Woods, S. Scypinski, L. J. Cline-Love, H. A. Ashworth, *Anal. Chem.* **1984**, *56*, 1395 – 1400.

[10] R. M. Ballew, J. N. Demas, *Anal. Chem.* **1989**, *61*, 30 – 33.

[11] K. K. Sharman, A. Periasamy, H. Ashworth, J. N. Demas, N. H. Snow, *Anal. Chem.* **1999**, *71*, 947 – 952.

[12] Y. Kostov, G. Rao, *Rev. Sci. Instrum.* **1999**, *70*, 4466 – 4470.

[13] S. G. Schulman, S. Chen, F. Bai, M. J. P. Leiner, L. Weis, O. S. Wolfbeis, *Anal. Chim. Acta* **1995**, *304*, 165 – 170.

[14] A. M. Paradiso, R. Y. Tsien, T. E. Machen, *Proc. Natl. Acad. Sci. USA* **1984**, *81*, 7436 – 7440.

[15] R. P. Haugland, *Handbook of Fluorescent Probes and Research Products*, Molecular Probes, Eugene, Oregon, **2002**; see http://probes.invitrogen.com/handbook/.

[16] a) B. J. Muller-Borer, H. Yang, S. A. Marzouk, J. J. Lemasters, W. E. Cascio, *Am. J. Physiol.* **1998**, *275(6 Pt 2)*, H1937 – 47; b) R. Sanders, A. Draaijer, H. C. Gerritsen, P. M. Houpt, Y. K. Levine, *Anal. Biochem.* **1995**, *227*, 302 – 308.

[17] J. W. Parker, O. Laksin, C. Yu, M. L. Lau, S. Klima, R. Fisher, I. Scott, B. W. Atwater, *Anal. Chem.* **1993**, *65*, 2329 – 2334.

[18] M. J. Boyer, D. W. Hedley, *Methods Cell Biol.* **1994**, *41*, 135 – 148.

[19] K. M. Hanson, M. J. Behne, N. P. Barry, T. M. Mauro, E. Gratton, R. M. Clegg, *Biophys. J.* **2002**, *83*, 1682 – 1690.

[20] C. Von Bültzingslöwen, A. K. McEnvoy, C. McDonagh, B. D. MacCraith, I. Klimant, C. Krause, O. S. Wolfbeis, *Analyst* **2002**, *127*, 1478 – 1483.

[21] K. Waich, T. Mayr, I. Klimant, *Talanta* **2008**, *77*, 66 – 72.

[22] C. Schröder, B. M. Weidgans, I. Klimant, *Analyst* **2005**, *130*, 907 – 916.

[23] H. Kautsky, A. Hirsch, *Z. Anorg. Allg. Chem.* **1935**, *222*, 126 – 134.

[24] a) T. Förster, *Ann. Phys.* **1948**, *437*, 55 – 75; b) M. Pineiro, A. L. Carvalho, M. M. Pereira, A. M. d'A. Rocha Gonsalves, L. G. Arnaut, S. J. Formosinho, *Chem. Eur. J.* **1998**, *4*, 2299 – 2307; c) E. Gross, D. Kovalev, N. Künzner, J. Diener, F. Koch, V. Y. Timoshenko, M. Fujii, *Phys. Rev. B* **2003**, *68*, 115405.

[25] a) J. Olmstedt III, *Chem. Phys. Lett.* **1974**, *26*, 33 – 36; b) F. Wilkinson, *Pure Appl. Chem.* **1997**, *69*, 851 – 856.

[26] D. L. Dexter, *J. Chem. Phys.* **1953**, *21*, 836 – 851.

[27] J. N. Demas, E. W. Harris, R. P. McBride, *J. Am. Chem. Soc.* **1977**, *99*, 3547 – 3551.

[28] C.-T. Lin, W. Bottcher, M. Chou, C. Creutz, N. Sutin, *J. Am. Chem. Soc.* **1976**, *98*, 6536 – 6544.

[29] a) "Luminescence Lifetime Imaging of Sensor Arrays": M. Schäferling in *Frontiers in Cehmical Sensors, Springer Series on Chemical Sensors and Biosensors*, *Vol. 3* (Eds.: G. Orellana, M. C. Moreno-Bondi), Springer, Berlin, **2005**, pp. 45 – 92; b) M. I. J. Stich, L. H. Fischer, O. S. Wolfbeis, *Chem. Soc. Rev.* **2010**, *39*, 3102 – 3114; c) S. M. Grist, L. Chrostowski, K. C. Cheung, *Sensors* **2010**, *10*, 9286 – 9316.

[30] a) S.-K. Lee, I. Okura, *Anal. Comm.* **1997**, *34*, 185 – 188; b) G. E. Khalil, M. Gouterman, S. Ching, C. Costin, L. Coyle, S. Gouin, E. Green, M. Sadilek, R. Wan, J. Yearyean, B. Zelelow, *J. Porphyrins Phthalocyanines* **2002**, *6*, 135 – 145; c) S. M. Borisov, I. Klimant, *Microchim. Acta* **2009**, *164*, 7 – 15.

[31] a) G. E. Khalil, C. Costin, J. Crafton, G. Jones, S. Grenoble, M. Gouterman, J. B. Callis, L. R. Dalton, *Sens. Actuators B* **2004**, *97*, 13 – 21; b) B. Zelelow, G. E. Khalil, G. Phelan, B. Carlson, M. Gouterman, J. B. Callis, L. R. Dalton, *Sens. Actuators B* **2003**, *96*, 304 – 314.

[32] D. B. Papkovsky, G. V. Ponomarev, W. Trettnak, P. O'Leary, *Anal. Chem.* **1995**, *67*, 4112 – 4117.

[33] a) J. E. Rogers, K. A. Nguyen, D. C. Hufnagle, D. G. McLean, W. Su, K. M. Gossett, A. R. Burke, S. A. Vinogradov, R. Pachter, P. A. Fleitz, *J. Phys. Chem. A* **2003**, *107*, 11331 – 11339; b) S. M. Borisov, G. Nuss, W. Haas, R. Saf, M. Schmuck, I. Klimant, *J. Photochem. Photobiol. A* **2009**, *201*, 128 – 135; c) C. Borek, K. Hanson, P. I. Djurovich, M. E. Thompson, K. Aznavour, R. Bau, Y. Sun, S. R. Forrest, J. Brooks, L. Michalski, J. Brown, *Angew. Chem.* **2007**, *119*, 1127 – 1130; *Angew. Chem. Int. Ed.* **2007**, *46*, 1109 – 1112.

[34] T. C. O'Riordan, A. V. Zhdanov, G. V. Ponomarev, D. B. Papkovsky, *Anal. Chem.* **2007**, *79*, 9414 – 9419.

[35] a) E. R. Carraway, J. N. Demas, B. A. DeGraff, J. R. Bacon, *Anal. Chem.* **1991**, *63*, 337 – 342; b) A. Mills, M. Thomas, *Analyst* **1997**, *122*, 63 – 68.

[36] a) G. Di Marco, M. Lanza, M. Pieruccini, S. Compagna, *Adv. Mater.* **1996**, *8*, 576 – 580; b) N. Tian, D. Lenkeit, S. Pelz, L. H. Fischer, D. Escudero, R. Schiewek, D. Klink, O. J. Schmitz, L. González, M. Schäferling, E. Holder, *Eur. J. Inorg. Chem.* **2010**, 4875 – 4885; c) Y. Amao, Y. Ishikawa, I. Okura, *Anal. Chim. Acta* **2001**, *445*, 177 – 182; d) M. E. Köse, R. J. Crutchley, M. C. DeRosa, N. Ananthakrishnan, J. R. Reynolds, K. S. Schanze, *Langmuir* **2005**, *21*, 8255 – 8262; e) S. M. Borisov, I. Klimant, *Anal. Chem.* **2007**, *79*, 7501 – 7509; f) C. S. K. Mak, D. Pentlehner, M. Stich, O. S. Wolfbeis, W. K. Chan, H. Yersin, *Chem. Mater.* **2009**, *21*, 2173 – 2175..

[37] C. Klein, R. H. Engler, U. Henne, W. E. Sachs, *Exp. Fluids* **2005**, *39*, 475 – 483.

[38] S. Nagl, C. Baleizão, S. M. Borisov, M. Schäferling, M. N. Berberan-Santos, O. S. Wolfbeis, *Angew. Chem.* **2007**, *119*, 2368 – 2371; *Angew. Chem. Int. Ed.* **2007**, *46*, 2317 – 2319.

[39] I. Klimant, R. Kühl, R. M. Glud, G. Holst, *Sens. Actuators B* **1997**, *38*, 29 – 37.

[40] D. B. Papkovsky, J. Olah, I. V. Troyanovsky, N. A. Sadovsky, V. D. Rumyantseva, A. F. Mironov, A. I. Yaropolov, A. P. Savitsky, *Biosens. Bioelectron.* **1992**, *7*, 199 – 206.

[41] Y. Amao, *Microchim. Acta* **2003**, *143*, 1 – 12.

[42] L. M. Coyle, M. Gouterman, *Sens. Actuators B* **1999**, *61*, 92 – 99.

[43] Z. Y. Zhang, K. T. V. Grattan, A. W. Palmer, *Rev. Sci. Instrum.* **1992**, *63*, 3869 – 3873.

[44] K. T. V. Grattan, Z. Y. Zhang, T. Sun, J. Shen, L. Tong, Z. Ding, *Meas. Sci. Technol.* **2001**, *12*, 981 – 986.

[45] Z. Y. Zhang, K. T. V. Grattan, *J. Lumin.* **1994**, *62*, 263 – 269.

[46] a) J. P. Feist, A. L. Heyes, S. Seefeldt, *Meas. Sci. Technol.* **2003**, *14*, N17; b) A. Omrane, G. Särner, M. Alden, *Appl. Phys. B* **2004**, *79*, 431 – 434.

[47] S. W. Allison, G. T. Gillies, *Rev. Sci. Instrum.* **1997**, *68*, 2615.

[48] S. M. Borisov, O. S. Wolfbeis, *Anal. Chem.* **2006**, *78*, 5094 – 5101.

[49] M. T. Berry, P. S. May, H. Xu, *J. Phys. Chem.* **1996**, *100*, 9216 – 9222.

[50] a) J. N. Demas, B. A. DeGraff, *Anal. Chem.* **1991**, *63*, 829A – 837A; b) G. Liebsch, I. Klimant, O. S. Wolfbeis, *Adv. Mater.* **1999**, *11*, 1296 – 1299.

[51] N. F. Mott, *Proc. R. Soc. London Ser. A* **1938**, *167*, 384 – 391.

[52] M. Poenie, J. Alderton, R. Y. Tsien, R. A. Steinhard, *Nature* **1985**, *315*, 147 – 149.

[53] a) R. B. Silver, *Methods Cell Biol.* **1998**, *56*, 237 – 251; b) T. Xu, W. Yang, X. L. Huo, T. Song, *J. Biochem. Biophys. Methods* **2004**, *58*, 219 – 226.

[54] G. Valet, A. Raffael, L. Rüssmann, *Naturwissenschaften* **1985**, *72*, 600 – 602.

[55] a) M. Oheim, M. Naraghi, T. H. Muller, E. Neher, *Cell Calcium* **1998**, *24*, 71 – 84; b) S. K. Lee, J. Y. Lee, M. Y. Lee, S. M. Chung, J. H. Chung, *Anal. Biochem.* **1999**, *273*, 186 – 191.

[56] a) X. P. Sun, N. Callamaras, J. S. Marchant, I. Parker, *J. Physiol.* **1998**, *509*, 67 – 80; b) Y. Ren, A. Ridsdale, E. Coderre, P. K. Stys, *J. Neurosci. Methods* **2000**, *102*, 165 – 176.

[57] O. Tour, S. R. Adams, R. A. Kerr, R. M. Meije, T. J. Sejnowski, R. W. Tsien, R. Y. Tsien, *Nat. Chem. Biol.* **2007**, *3*, 423 – 431.
[58] A. Minta, J. P. Kao, R. Y. Tsien, *J. Biol. Chem.* **1989**, *264*, 8171 – 8178.
[59] G. R. Budinger, J. Duranteau, N. S. Chandel, P. T. Schumacker, *J. Biol. Chem.* **1998**, *273*, 3320 – 3326.
[60] K. Meuwis, N. Boens, F. C. De Schryver, J. Gallay, M. Vincent, *Biophys. J.* **1995**, *68*, 2469 – 2473.
[61] A. Minta, R. Y. Tsien, *J. Biol. Chem.* **1989**, *264*, 19449 – 19457.
[62] M. M. Henary, Y. Wu, C. J. Fahrni, *Chem. Eur. J.* **2004**, *10*, 3015 – 3025.
[63] N. Strömberg, S. Hulth, *Sens. Actuators B* **2003**, *90*, 308 – 318.
[64] A. Weller, *Pure Appl. Chem.* **1968**, *16*, 115 – 123.
[65] G. L. Closs, J. R. Miller, *Science* **1988**, *240*, 440 – 447.
[66] A. P. de Silva, T. Gunnlaugsson, T. E. Rice, *Analyst* **1996**, *121*, 1759 – 1762.
[67] A. P. de Silva, H. Q. N. Gunaratne, T. Gunnlaugsson, A. J. M. Huxley, C. P. McCoy, J. T. Rademacher, T. E. Rice, *Chem. Rev.* **1997**, *97*, 1515 – 1566.
[68] H. He, M. A. Mortellaro, M. J. P. Leiner, R. J. Fraatz, J. K. Tusa, *J. Am. Chem. Soc.* **2003**, *125*, 1468 – 1469.
[69] http://www.optimedical.com.
[70] F. R. Richardson, *Chem. Rev.* **1982**, *82*, 541 – 552.
[71] D. Parker, R. S. Dickins, H. Puschmann, C. Crossland, J. A. K. Howard, *Chem. Rev.* **2002**, *102*, 1977 – 2010.
[72] a) J. Georges, *Analyst* **1993**, *118*, 1481 – 1486; b) C. M. G. Dos Santos, A. J. Harte, S. J. Quinn, T. Gunnlaugsson, *Coord. Chem. Rev.* **2008**, *252*, 2512 – 2527.
[73] a) A. Dadabhoy, S. Faulkner, P. G. Sammes, *J. Chem. Soc. Perkin Trans. 2* **2000**, 2359 – 2360; b) A. Beeby, L. M. Bushby, D. Maffeo, J. A. G. Williams, *J. Chem. Soc. Perkin Trans. 2* **2000**, 1281 – 1283.
[74] D. Parker, *Coord. Chem. Rev.* **2000**, *205*, 109 – 130.
[75] a) M. S. Tremblay, D. Sames, *Chem. Commun.* **2006**, 4116 – 4118; b) J. P. Leonard, C. B. Nolan, F. Stomeo, T. Gunnlaugsson, *Top. Curr. Chem.* **2007**, *281*, 1 – 43.
[76] T. Gunnlaugsson, C. P. McCoy, F. Stomeo, *Tetrahedron Lett.* **2004**, *45*, 8403 – 8407.
[77] T. Gunnlaugsson, J. P. Leonard, K. Senecal, A. J. Harte, *J. Am. Chem. Soc.* **2003**, *125*, 12062 – 12063.
[78] T. Gunnlaugsson, J. P. Leonard, *Chem. Commun.* **2003**, 2424 – 2425.
[79] S. J. A. Pope, R. H. Laye, *J. Chem. Soc. Dalton Trans.* **2006**, 3108 – 3113.
[80] a) J.-C. G. Bünzli, *Chem. Rev.* **2010**, *110*, 2729 – 2755; b) I. Hemmilä, V. Laitala, *J. Fluoresc.* **2005**, *15*, 529 – 542; c) N. Sabbatini, M. Guardigli, J.-M. Lehn, *Coord. Chem. Rev.* **1993**, *123*, 201 – 228.
[81] a) O. S. Wolfbeis, A. Duerkop, M. Wu, Z. Lin, *Angew. Chem.* **2002**, *114*, 4681 – 4684; *Angew. Chem. Int. Ed.* **2002**, *41*, 4495 – 4498; b) M. Schäferling, M. Wu, J. Enderlein, H. Bauer, O. S. Wolfbeis, *Appl. Spectrosc.* **2003**, *57*, 1386 – 1392.
[82] F. Hou, Y. Miao, C. Jiang, *Spectrochim. Acta Part A* **2005**, *61*, 2891 – 2895.
[83] C. Spangler, C. M. Spangler, M. Spoerner, M. Schäferling, *Anal. Bioanal. Chem.* **2009**, *394*, 989 – 996.
[84] A. Duerkop, M. Turel, A. Lobnik, O. S. Wolfbeis, *Anal. Chim. Acta* **2006**, *555*, 292 – 298.
[85] Z. Lin, M. Wu, M. Schäferling, O. S. Wolfbeis, *Angew. Chem.* **2004**, *116*, 1767 – 1770; *Angew. Chem. Int. Ed.* **2004**, *43*, 1735 – 1738.
[86] a) C. Jiang, L. Luo, *Anal. Chim. Acta* **2004**, *551*, 11 – 16; b) C. Jiang, L. Luo, *Anal. Chim. Acta* **2004**, *506*, 171 – 175; c) X. Zhu, X. Wang, C. Jiang, *Anal. Biochem.* **2005**, *341*, 299 – 307.
[87] A. V. Yegorova, Y. V. Scripinets, A. Duerkop, A. A. Karasyov, V. P. Antonovich, O. S. Wolfbeis, *Anal. Chim. Acta* **2007**, *584*, 260 – 267.
[88] a) C. M. Spangler, C. Spangler, M. Göttle, Y. Shen, W.-J. Tang, R. Seifert, M. Schäferling, *Anal. Biochem.* **2008**, *381*, 86 – 93; b) M. Schäferling, O. S. Wolfbeis, *Chem. Eur. J.* **2007**, *13*, 4342 – 4349; c) C. M. Spangler, C. Spangler, M. Schäferling, *Ann. N. Y. Acad. Sci.* **2008**, *1130*, 138 – 148.
[89] "Luminescent Chemical and Physical Sensors Based on Lanthanide Complexes": C. M. Spangler, M. Schäferling in *Springer Series on Fluorescence*, *Vol. 7* (Eds.: P. Hänninen, H. Härmä), Springer, Berlin, **2011**, pp. 235 – 262.
[90] a) W. Lian, S. A. Litherland, H. Badrane, W. Tan, D. Wu, H. V. Baker, P. A. Gulig, D. V. Lim, S. Jin, *Anal. Biochem.* **2004**, *334*, 135 – 144; b) L. Kokko, T. Lovgren, T. Soukka, *Anal. Chim. Acta* **2007**, *585*, 17 – 23.
[91] T. Behnke, C. Würth, K. Hoffmann, M. Hübner, U. Panne, U. Resch-Genger, *J. Fluoresc.* **2011**, *21*, 937 – 944.
[92] J. M. Kürner, I. Klimant, C. Krause, H. Preu, W. Kunz, O. S. Wolfbeis, *Bioconjugate Chem.* **2001**, *12*, 883 – 889.
[93] "Biopolymer and polymer nanoparticles and their biomedical applications": E. Nakache, N. Poulain, F. Candau, A.-M. Orecchioni, J. M. Irache in *Handbook of Nanostructured Materials and Nanotechnology*, *Vol. 5* (Ed.: H. S. Nalwa), Academic Press, San Diego, **2000**, pp. 577 – 635.
[94] a) J. F. Bringley, T. L. Penner, R. Wang, J. F. Harder, W. J. Harrison, L. Buonemani, *J. Colloid Interface Sci.* **2008**, *320*, 132 – 139; b) S. Bonacchi, D. Genovese, R. Juris, M. Montalti, L. Prodi, E. Rampazzo, N. Zaccheroni, *Angew. Chem.* **2011**, *123*, 4142 – 4152; *Angew. Chem. Int. Ed.* **2011**, *50*, 4056 – 4066.
[95] a) I. Miletto, A. Gilardino, P. Zamburlin, S. Dalmazzo, D. Lovisolo, G. Caputo, G. Viscardi, G. Martra, *Dyes Pigm.* **2009**, *84*, 121 – 127; b) E. Herz, H. Ow, D. Bonner, A. Burns, U. Wiesner, *J. Mater. Chem.* **2009**, *19*, 6341 – 6347.
[96] S. Santra, P. Zhang, K. Wang, R. Tapec, W. Tan, *Anal. Chem.* **2001**, *73*, 4988 – 4993.
[97] I. Klimant, F. Ruckruh, G. Liebsch, A. Stangelmayer, O. S. Wolfbeis, *Microchim. Acta* **1999**, *131*, 35 – 46.
[98] a) Y. E. K. Lee, R. Kopelman, *Wiley Interdiscip. Rev. Nanomed. Nanobiotechnol.* **2009**, *1*, 98 – 110; b) S. M. Borisov, I. Klimant, *Analyst* **2008**, *133*, 1302 – 1307.
[99] Y. Cao, Y.-E. L. Koo, R. Kopelman, *Analyst* **2004**, *129*, 745 – 750.
[100] Y.-E. L. Koo, Y. Cao, R. Kopelman, S. M. Koo, M. Brasuel, M. A. Philbert, *Anal. Chem.* **2004**, *76*, 2498 – 2505.
[101] X.-d. Wang, H. H. Gorris, J. A. Stolwijk, R. J. Meier, D. B. M. Groegel, J. Wegener, O. S. Wolfbeis, *Chem. Sci.* **2011**, *2*, 901 – 906.
[102] J. P. Sumner, N. M. Westerberg, A. K. Stoddard, C. A. Fierke, R. Kopelman, *Sens. Actuators B* **2006**, *113*, 760 – 767.
[103] H.-s. Peng, J. A. Stolwijk, L.-N. Sun, J. Wegener, O. S. Wolfbeis, *Angew. Chem.* **2010**, *122*, 4342 – 4345; *Angew. Chem. Int. Ed.* **2010**, *49*, 4246 – 4249.
[104] R. M. Sánchez-Martín, M. Cuttle, S. Mittoo, M. Bradley, *Angew. Chem.* **2006**, *118*, 5598 – 5600; *Angew. Chem. Int. Ed.* **2006**, *45*, 5472 – 5474.
[105] G. Kim, Y.-E. K. Lee, H. Xu, M. A. Philbert, R. Kopelman, *Anal. Chem.* **2010**, *82*, 2165 – 2169.
[106] Y.-E. K. Lee, E. E. Ulbrich, G. Kim, H. Hah, C. Strollo, W. Fan, R. Gurjar, S. M. Koo, R. Kopelman, *Anal. Chem.* **2010**, *82*, 8446 – 8455.
[107] J. Napp, T. Behnke, L. Fischer, C. Würth, M. Wottawa, D. M. Katschinski, F. Alves, U. Resch-Genger, M. Schäferling, *Anal. Chem.* **2011**, *83*, 9039 – 9046.
[108] a) A. Burns, P. Sengupta, T. Zedayko, B. Baird, U. Wiesner, *Small* **2006**, *2*, 723 – 726; b) A. Burns, H. Ow, U. Wiesner, *Chem. Soc. Rev.* **2006**, *35*, 1028 – 1042; c) Y. Piao, A. Burns, J. Kim, U. Wiesner, T. Hyeon, *Adv. Funct. Mater.* **2008**, *18*, 3745 – 3758.

[109] A. Burns, J. Vider, H. Ow, E. Herz, O. Penate-Medina, M. Baumgart, S. m. Larson, U. Wiesner, M. Bradbury, *Nano Lett.* **2009**, *9*, 442 – 448.
[110] Z. Li, Y. Zhang, S. Jiang, *Adv. Mater.* **2008**, *20*, 4765 – 4769.
[111] a) N. R. Jana, C. Earhart, J. Y. Ying, *J. Mater. Chem.* **2007**, *19*, 5074 – 5082; b) T. Nann, P. Mulvaney, *Angew. Chem.* **2004**, *116*, 5511 – 5514; *Angew. Chem. Int. Ed.* **2004**, *43*, 5393 – 5396.
[112] H. Peng, M. I. J. Stich, J. Yu, L.-n. Sun, L. H. Fischer, O. S. Wolfbeis, *Adv. Mater.* **2010**, *22*, 716 – 719.
[113] S. Gu, T. Kondo, M. Konno, *J. Colloid Interface Sci.* **2004**, *272*, 314 – 320.
[114] Z. Li, G. Liu, *Biomacromolecules* **2002**, *3*, 984 – 990.
[115] L. H. Fischer, S. M. Borisov, M. Schäferling, I. Klimant, O. S. Wolfbeis, *Analyst* **2010**, *135*, 1224 – 1229.
[116] N. L. Rochefort, H. Jia, A. Konnerth, *Trends Mol. Med.* **2008**, *14*, 389 – 399.
[117] T. Bagar, K. Altenbach, N. D. Read, M. Bencina, *Eukaryotic Cell* **2009**, *8*, 703 – 712.
[118] a) V. V. Belousov, a. F. Fradkov, K. A. Lukyanov, D. B. Staroverov, K. S. Shakhbazov, A. V. Terskikh, S. Lukyanov, *Nat. Methods* **2006**, *3*, 281 – 286; b) D. Lee, S. Khaja, J. C. Velasquez-Castano, M. Dasari, C. Sun, J. Petros, W. R. Taylor, N. Murthy, *Nat. Mater.* **2007**, *6*, 765 – 769; c) P. Niethammer, C. Grabher, A. T. Look, T. J. Mitchison, *Nature* **2009**, *459*, 996 – 999; d) B. C. Dickinson, C. Huynh, C. J. Chang, *J. Am. Chem. Soc.* **2010**, *132*, 5906 – 5915.
[119] O. S. Wolfbeis, *Adv. Mater.* **2008**, *20*, 3759 – 3763.
[120] J. I. Peterson, R. V. Fitzgerald, *Rev. Sci. Instrum.* **1980**, *51*, 670 – 671.
[121] J. H. Bell, E. T. Schairer, L. A. Hand, R. D. Mehta, *Annu. Rev. Fluid Mech.* **2001**, *33*, 155 – 206.
[122] a) R. H. Engler, M. C. Merienne, C. Klein, Y. Le Sant, *Aerosp. Sci. Technol.* **2002**, *6*, 313 – 322; b) K. Asai, Y. Amao, Y. Iijima, I. Okura, H. Nishide, *J. Thermophys. Heat Transfer* **2002**, *16*, 109 – 115.
[123] T. Liu, J. P. Sullivan, *Pressure and Temperature Sensitive Paints*, Springer, Berlin, **2005**.
[124] B. G. McLachlan, J. H. Bell, J. Espina, J. Gallery, M. Gouterman, C. G. N. Demandante, L. Bjarke, NASA Technical Memorandum 103970, **1992**.
[125] S. Draxler, M. E. Lippitsch, I. Klimant, H. Kraus, O. S. Wolfbeis, *J. Phys. Chem.* **1995**, *99*, 3162 – 3176.
[126] "Permeation and Diffusion Data": S. Pauly in *Polymer Handbook*, 4th ed. (Eds.: J. Brandrup, E. H. Immergut, E. H. Gruhlke), Wiley, New York, **1999**, pp. 543 – 569.
[127] P. Y. Hsieh, *J. Appl. Polym. Sci.* **1963**, *7*, 1743 – 1756.
[128] S. A. Stern, V. M. Shah, B. J. Hardy, *J. Polym. Sci. Part B* **1987**, *25*, 1263 – 1298.
[129] E. Puklin, B. Carlson, S. Gouin, C. Costin, E. Green, S. Ponomarev, H. Tanji, M. Gouterman, *J. Appl. Polym. Sci.* **2000**, *77*, 2795 – 2804.
[130] M. Kameda, T. Tabei, K. Nakakita, H. Sakaue, K. Asai, *Meas. Sci. Technol.* **2005**, *16*, 2517 – 2524.
[131] J. N. Demas, B. A. DeGraff, W. Xu, *Anal. Chem.* **1995**, *67*, 1377 – 1380.
[132] C. Baleizão, S. Nagl, S. Borisov, M. Schäferling, O. S. Wolfbeis, M. N. Berberan-Santos, *Chem. Eur. J.* **2007**, *13*, 3643 – 3651.
[133] J. R. Kingsley-Rowe, G. D. Lock, A. G. Davies, *Aeronaut. J.* **2003**, *107*, 649 – 656.
[134] P. Vaupel, F. Kallinowski, P. Okunieff, *Cancer Res.* **1989**, *49*, 6449 – 6465.
[135] a) I. Dunphy, S. A. Vinogradov, D. F. Wilson, *Anal. Biochem.* **2002**, *310*, 191 – 198; b) L. S. Ziemer, W. M. F. Lee, S. A. Vinogradov, C. Sehgal, D. F. Wilson, *J. Appl. Physiol.* **2005**, *98*, 1503 – 1510.
[136] S. Zhang, M. Hosaka, T. Yoshihara, K. Negishi, Y. Iida, S. Tobita, T. Takeuchi, *Cancer Res.* **2010**, *70*, 4490 – 4498.
[137] a) P. Babilas, V. Schacht, G. Liebsch, O. S. Wolfbeis, M. Landthaler, R.-M. Szeimies, C. Abels, *Br. J. Cancer* **2003**, *88*, 1462 – 1469; b) P. Babilas, G. Liebsch, V. Schacht, I. Klimant, O. S. Wolfbeis, R.-M. Szeimies, C. Abels, *Microcirculation* **2005**, *12*, 477 – 487.
[138] S. Kellner, G. Liebsch, I. Klimant, O. S. Wolfbeis, T. Blunk, M. B. Schulz, A. Göpferich, *Biotechnol. Bioeng.* **2002**, *80*, 73 – 83.
[139] O. S. Wolfbeis, *J. Mater. Chem.* **2005**, *15*, 2657 – 2669.
[140] G. Liebsch, I. Klimant, C. Krause, O. S. Wolfbeis, *Anal. Chem.* **2001**, *73*, 4354 – 4363.
[141] S. Schreml, R. J. Meier, O. S. Wolfbeis, M. Landthaler, R.-M. Szeimies, P. Babilas, *Proc. Natl. Acad. Sci. USA* **2011**, *108*, 2432 – 2437.
[142] a) E. Precht, U. Franke, L. Polerecky, M. Huettel, *Limnol. Oceanogr.* **2004**, *49*, 693 – 705; b) R. N. Glud, F. Wenzhoefer, A. Tengberg, M. Middelboe, K. Oguri, H. Kitazato, *Deep-Sea Res. Part I* **2005**, *52*, 1974 – 1987.
[143] U. Franke, L. Polerecky, E. Precht, M. Huettel, *Limnol. Oceanogr.* **2006**, *51*, 1084 – 1096.
[144] L. Polerecky, N. Volkenborn, P. Stief, *Environ. Sci. Technol.* **2006**, *40*, 5763 – 5769.
[145] K. Oguri, H. Kitazato, R. N. Glud, *Mar. Chem.* **2006**, *100*, 95 – 107.
[146] a) M. Kühl, L. Polerecky, *Aquat. Microb. Ecol.* **2008**, *53*, 99 – 118; b) R. N. Glud, H. Stahl, P. Berg, F. Wenzhoefer, K. Oguri, H. Kitazato, *Limnol. Oceanogr.* **2009**, *54*, 1 – 12.
[147] a) W. Trettnak, M. J. P. Leiner, O. S. Wolfbeis, *Analyst* **1988**, *113*, 1519 – 1523; b) L. Li, D. R. Walt, *Anal. Chem.* **1995**, *67*, 3746 – 3752.
[148] M. I. J. Stich, S. Nagl, O. S. Wolfbeis, U. Henne, M. Schäferling, *Adv. Funct. Mater.* **2008**, *18*, 1399 – 1406.
[149] E. Holder, B. M. W. Langeveld, U. S. Schubert, *Adv. Mater.* **2005**, *17*, 1109 – 1121.
[150] a) Y. Amao, Y. Ishikawa, I. Okura, *Anal. Chim. Acta* **2001**, *445*, 177 – 182; b) A. L. Medina-Castillo, J. F. Fernandez-Sanchez, C. Klein, M. K. Nazeeruddin, A. Segura-Carretero, A. Fernandez-Guiterrez, M. Graetzel, U. E. Spichiger-Keller, *Analyst* **2007**, *132*, 929 – 936; c) D. Di Marco, M. Lanza, A. Mamo, I. Stefio, C. Di Pietro, G. Romero, S. Campagna, *Anal. Chem.* **1998**, *70*, 5019 – 5023.
[151] L. H. Fischer, M. I. J. Stich, O. S. Wolfbeis, N. Tian, E. Holder, M. Schäferling, *Chem. Eur. J.* **2009**, *15*, 10857 – 10863.
[152] J. Hradil, C. Davis, K. Mongey, C. McDonagh, B. D. MacCraith, *Meas. Sci. Technol.* **2002**, *13*, 1552 – 1557.
[153] M. E. Köse, B. F. Carroll, K. S. Schanze, *Langmuir* **2005**, *21*, 921 – 929.
[154] S. M. Borisov, A. S. Vasylevska, C. Krause, O. S. Wolfbeis, *Adv. Funct. Mater.* **2006**, *16*, 1536 – 1542.
[155] C. Baleizão, S. Nagl, M. Schäferling, M. N. Berberan-Santos, O. S. Wolfbeis, *Anal. Chem.* **2008**, *80*, 6449 – 6457.
[156] O. S. Wolfbeis, L. J. Weis, M. J. P. Leiner, W. E. Ziegler, *Anal. Chem.* **1988**, *60*, 2028 – 2030.
[157] S. M. Borisov, C. Krause, S. Arain, O. S. Wolfbeis, *Adv. Mater.* **2006**, *18*, 1511 – 1516.
[158] G. S. Vasylevska, S. M. Borisov, C. Krause, O. S. Wolfbeis, *Chem. Mater.* **2006**, *18*, 4609 – 4616.
[159] A. S. Kocincová, S. Nagl, S. Arain, C. Krause, S. M. Borisov, M. Arnold, O. S. Wolfbeis, *Biotechnol. Bioeng.* **2008**, *100*, 430 – 438.
[160] C. R. Schröder, G. Neurauter, I. Klimant, *Microchim. Acta* **2007**, *158*, 205 – 218.
[161] C. R. Schröder, L. Polerecky, I. Klimant, *Anal. Chem.* **2007**, *79*, 60 – 70.
[162] R. J. Meier, S. Schreml, X.-d. Wang, M. Landthaler, P. Babilas, O. S. Wolfbeis, *Angew. Chem.* **2011**, *123*, 11085—11088; *Angew. Chem. Int. Ed.* **2011**, *50*, 10893—10896.

[163] M. I. J. Stich, S. M. Borisov, U. Henne, M. Schäferling, *Sens. Actuators B* **2009**, *139*, 204 – 207.
[164] S. M. Borisov, K. Gatterer, I. Klimant, *Analyst* **2010**, *135*, 1711 – 1717.
[165] C. Pietsch, R. Hoogenboom, U. S. Schubert, *Angew. Chem.* **2009**, *121*, 5763 – 5766; *Angew. Chem. Int. Ed.* **2009**, *48*, 5653 – 5656.
[166] S. M. Borisov, R. Seifner, I. Klimant, *Anal. Bioanal. Chem.* **2011**, *400*, 2463 – 2474.
[167] W. W. Miller, M. Yafuso, C. F. Yan, H. K. Hui, S. Arick, *Clin. Chem.* **1987**, *33*, 1538 – 1542.
[168] M. I. J. Stich, M. Schäferling, O. S. Wolfbeis, *Adv. Mater.* **2009**, *21*, 2216 – 2220.
[169] A. J. Palma, J. López-González, L. J. Asensio, M. D. Fernández-Ramos, L. F. Capitán-Vallvey, *Sens. Actuators B* **2007**, *121*, 629 – 638.
[170] S. Nagl, M. I. J. Stich, M. Schäferling, O. S. Wolfbeis, *Anal. Bioanal. Chem.* **2009**, *393*, 1199 – 1207.
[171] J. Enderlein, M. Sauer, *J. Phys. Chem. A* **2001**, *105*, 48 – 53.
[172] M. Grabolle, P. Kapusta, T. Nann, X. Shu, J. Ziegler, U. Resch-Genger, *Anal. Chem.* **2009**, *81*, 7807 – 7813.
[173] X.-d. Wang, R. J. Meier, M. Link, O. S. Wolfbeis, *Angew. Chem.* **2010**, *122*, 5027 – 5029; *Angew. Chem. Int. Ed.* **2010**, *49*, 4907 – 4909.
[174] A. Martinez-Olmos, S. Capel-Cuevas, N. López-Ruiz, A. J. Palma, I. de Orbe, L. F. Capitán-Vallvey, *Sens. Actuators B* **2011**, *156*, 840 – 848.
[175] B. Valuer, *Molcular Fluorescence*, Wiley-VCH, Weinheim, **2000**.
[176] J. R. Lakowicz, *Principles of Fluorescence Spectroscopy*, 3rd ed., Springer, New York, **2006**.
[177] A. P. Demchenko, *Introduction to Fluorescence Sensing*, Springer, Berlin, **2009**.
[178] "Boronic Acid-Based Fluorescence Sensors for Glucose Monitoring": G. Kaur, N. Lin, H. Fang, B. Wang in *Topics in Fluorescence Spectroscopy*, *Vol. 11* (Eds.: C. D. Geddes, J. R. Lakowicz, Jr.), Springer, New York, **2006**, pp. 377 – 397.
[179] a) E. W. Miller, O. Tulyathan, E. Y. Isacoff, C. J. Chang, *Nat. Chem. Biol.* **2007**, *3*, 263 – 267; b) D. Srikun, A. E. Albers, C. I. Nam, A. T. IavaroneT, C. J. Chang, *J. Am. Chem. Soc.* **2010**, *132*, 4455 – 4465; c) E. W. Miller, B. C. Dickinson, C. J. Chang, *Proc. Natl. Acad. Sci. USA* **2010**, *107*, 15681 – 15686; d) H. Maeda, Y. Fukuyasu, S. Yoshida, M. Fukuda, K. Saeki, H. Matsuno, Y. Yamauchi, K. Yoshida, K. Hirata, K. Miyamoto, *Angew. Chem.* **2004**, *116*, 2443 – 2445; *Angew. Chem. Int. Ed.* **2004**, *43*, 2389 – 2391.
[180] A. Ojida, S.-k. Park, Y. Mito-oka, I. Hamachi, *Tetrahedron Lett.* **2002**, *43*, 6193 – 6195.
[181] a) P. D. Beer, P. A. Gale, *Angew. Chem.* **2001**, *113*, 502 – 532; *Angew. Chem. Int. Ed.* **2001**, *40*, 486 – 516; b) R. Martinez-Máñez, F. Sancenón, *Chem. Rev.* **2003**, *103*, 4419 – 4476; c) J. Biwersi, B. Tulk, A. S. Verlman, *Anal. Biochem.* **1994**, *219*, 139 – 143.
[182] K. Kiyose, H. Kojima, T. Nagano, *Chem. Asian J.* **2008**, *3*, 506 – 515.
[183] L. H. Fischer, G. S. Harms, O. S. Wolfbeis, *Angew. Chem.* **2011**, *123*, 4640 – 4645; *Angew. Chem. Int. Ed.* **2011**, *50*, 4546 – 4551.
[184] D. Filippini, A. Alimelli, C. Di Natale, R. Paolesse, A. D'Amico, I. Lundström, *Angew. Chem.* **2006**, *118*, 3884 – 3887; *Angew. Chem. Int. Ed.* **2006**, *45*, 3800 – 3803.
[185] a) S. H. Lim, L. Feng, J. W. Kemling, C. J. Musto, K. S. Suslick, *Nat. Chem.* **2009**, *1*, 562 – 567; M. M. Erenas, M. C. Pegalajar, M. P. Cuellar, I. de Orbe-Payá, L. F. Capitán-Vallvey, *Sens. Actuators B* **2011**, *156*, 976 – 982.
[186] a) Z. Iqbal, D. Filippini, *J. Sensors* **2010**, Article ID 381796; b) A. García, M. M. Erenas, E. D. Marinetto, C. A. Abad, I. de Orbe-Paya, A. J. Palma, L. F. Capitán-Vallvey, *Sens. Actuators B* **2011**, *156*, 350 – 359.

